A green lifetime biosensor for calcium that remains bright over its full dynamic range

Franka H. van der Linden[1], Stephen C. Thornquist[2], Rick M. ter Beek[1], Jelle Y. Huijts[1], Mark A. Hink[1], Theodorus W.J. Gadella Jr. [1] , Gaby Maimon[2], & Joachim Goedhart[1,*]

Affiliations:
[1]Swammerdam Institute for Life Sciences, Section of Molecular Cytology, van Leeuwenhoek Centre for Advanced Microscopy, University of Amsterdam, Amsterdam, the Netherlands.
[2]Laboratory of Integrative Brain Function and Howard Hughes Medical Institute, The Rockefeller University, New York, NY, USA

[*]Correspondence: j.goedhart@uva.nl

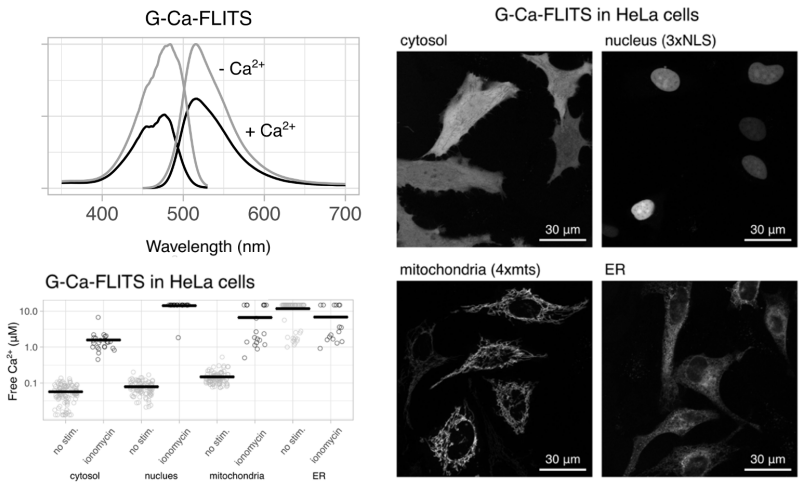

Abstract

Fluorescent biosensors toggle between two states and for the vast majority of biosensors one state is bright and the other state is dim. As a consequence, there is a substantial difference in the signal-to-noise ratio (SNR) for the two states. The dim state has a low signal-to-noise ratio, which is problematic when precise, quantitative measurements are needed. During the engineering of a red-shifted variant of an mTurquoise-based calcium sensor, we serendipitously generated a green-emitting sensor that shows high brightness in both the calcium-bound and -unbound state, while still showing a calcium dependent lifetime change of >1 nanosecond. This sensor, named G-Ca-FLITS, is comparable in brightness to the bright state of GCaMP3 and jGCaMP7c in mammalian cells. The calcium induced loss in fluorescence intensity is only around 30% and therefore we observe little variation in the SNR when calcium levels change. G-Ca-FLITS shows negligible sensitivity to pH in the physiological range, like its turquoise parent. Using fluorescence lifetime imaging (FLIM), we measured the calcium concentration with G-Ca-FLITS in various organelles and observed in HeLa cells transient and spatially heterogeneous calcium elevations in mitochondria. Finally, we evaluated the use of G-Ca-FLITS and its turquoise predecessor for two-photon FLIM in *Drosophila* brains.

Introduction

Genetically Encoded Calcium Indicators (GECIs) are by far the largest family of biosensors, with over 100 members (Greenwald et al., 2018) including the well-known GCaMP series. Many GECIs harboring a single fluorescent protein (FP), like GCaMPs, are optimized for a large intensity change, and have a (very) dim state when calcium levels are below the K_D of the probe (Akerboom et al., 2013; Dana et al., 2019; Shen et al., 2018; Zhang et al., 2023; Zhao et al., 2011). Additionally, the fluorescence of most sensors is a non-linear function of calcium concentration, usually with Hill coefficients between 2 and 3. This is ideal when the probe is used as a binary detector for increases in Ca^{2+} concentrations, but it makes robust quantification of low, or even intermediate, calcium concentrations extremely challenging. For precise quantification of low calcium concentrations a biosensor with an inverted response (Barykina et al., 2016) is a good alternative, as these variants are bright in the calcium-free state. However, this only partially resolves the issue, reducing the precision of measurements for the conditions where the calcium concentration exceeds the K_D of the probe.

The fluorescence intensity is affected by many factors (Culley et al., 2024; Waters, 2009), complicating the measurement of absolute calcium concentrations with biosensors that use intensity contrast as a read-out. Therefore, we and others have engineered genetically encoded biosensors that use other read-outs. New biosensors that report with a change in photochromic behaviour (Bierbuesse et al., 2022), anisotropy (Laskaratou et al., 2021), or fluorescence lifetime (Díaz-García et al., 2017; Klarenbeek et al., 2015; van der Linden et al., 2021) have been developed. In all these approaches the precision of the measurement depends on the number of emitted photons. The turquoise lifetime sensor Tq-Ca-FLITS that we developed (van der Linden et al., 2021) shows a 3-fold intensity change, with the low intensity (and low SNR) at low calcium concentrations. To better measure both states accurately, i.e., with high SNR, one would want a biosensor that is bright in both states. Such a sensor could be used for imaging low concentrations of calcium and subsequent increases, for example in various organelles of unstimulated mammalian cells, including mitochondria (Parry et al., 2024).

Calcium signaling in mitochondria is reported to be linked with several pathophysiological processes including inflammatory responses, diabetes, heart failure, neurological diseases and cancer (Delierneux et al., 2020; Giorgi et al., 2018). Over the years, mitochondrial calcium concentrations have been measured with imaging techniques; however, there are discrepancies between the reported values. The affinity of a sensor is of major importance: a low K_D can underestimate high concentrations and vice versa. Differences can also arise due to the method of calibration, i.e. when the absolute minimum and maximum signal are not reached in the calibration procedure (Fernandez-Sanz et al., 2019). Also, the sensor's kinetics should be sufficiently fast enough to be able to follow the calcium changes. Aside from the previously discussed fluorescent biosensors, imaging has also been performed with fluorescent calcium dyes (Rhod-2) and aequorin bioluminescent sensors. However, fluorescent calcium dyes appear to have difficulties following repetitive imaging in comparison to protein-based biosensors and morphological changes to cells are observed, especially after light exposure (Fonteriz et al., 2010) . Also, fluorescent dyes are difficult to target to mitochondria, so cytoplasmic signals can easily contaminate the measurements. Bioluminescence sensors are unfavorable when cell-to-cell variation is

studied due to their low signal intensity, which hinders single cell imaging. Finally, regardless of the biosensor that is used, it should give a stable signal at the high mitochondrial pH of 8 (Cano Abad et al., 2004; Llopis et al., 1998).

Clearly, there is a need for robust calcium sensors that perform well in all criteria discussed above. In this paper we document the development of a green calcium sensor by an optimized bacterial screening method. We report the spectroscopic properties of the purified sensor and show its use for robust measurements of calcium levels in mitochondria of HeLa cells and endothelial cells by lifetime imaging.

RESULTS

A high throughput method to screen sensors in bacterial lysate

Before creating sensor variants, we developed a high-throughput method to screen different calcium sensors in bacterial lysate. The aim was to grow and isolate 96 bacterial cultures in parallel in a deep well plate. A previously developed lysis buffer (Danilevich et al., 2008) served as a starting point for optimization of the protocol. Bacteria expressing the sensor Tq-Ca-FLITS were used to compare the lysis efficiency. The following variables were tested in a 50 mM Tris-HCl buffer: 1) presence or absence of a freeze/thawing cycle, 2) presence or absence of lysozyme, 3) different concentrations of urea (0, 0.5 and 1 M), 4) different concentrations of deoxycholic acid (DOC, 1, 2 and 3%). After lysis, the fluorescence intensity of the bacterial lysates was compared (Figure S1).

In general, a freezing and thawing cycle resulted in a higher fluorescence intensity for most conditions. However, this doubled the duration of the protocol. A high concentration of DOC and urea combined was too harsh for the fluorescent sensor: no intensity was detected. All other conditions were comparable. We favored a buffer without urea to maintain the native state of the proteins, and without lysozyme to omit the need to freshly add this component before each use. Therefore, we chose a protocol with 2% DOC and without a freezing step. The obtained lysates were of sufficient brightness and purity to use for spectral measurements and lifetime measurements.

We explored the possibility of replacing the 2% DOC with other detergents, but no improvements were found. Triton-X100 (0.1-1%) gave lower intensities compared to DOC and caused a problematic amount of foam during handling. Sodium dodecyl sulfate (SDS, 0.1-0.5%), an anionic surfactant in contrast to non-ionic Triton-X100 and DOC, also gave lower intensities and poses the risk of denaturation of the proteins (Figure S2). Therefore, we chose the 50 mM Tris-HCl buffer with 2% DOC for further experiments.

Creating a red shifted calcium sensor with lifetime contrast

We aimed to generate a green biosensor with lifetime contrast. Therefore, we used the previously developed turquoise sensor (Tq-Ca-FLITS) and mutated residues that potentially induce a red-shift. We subjected the Tq-Ca-FLITS to directed mutagenesis of residues T203 (mTurquoise2 numbering, T81 in the full sensor) and I167 (mTurquoise2 numbering, I45 in the full sensor) to aromatic amino acids. Both residues are located close to the chromophore. The mutation T203Y is known to cause a red shift in green fluorescent proteins (Ormö et al., 1996) and mTurquoise2 (Gorbachev et al., 2017). We anticipated that π-π stacking of the aromatic residue with the chromophore would result in the color shift in Tq-Ca-FLITS as well. The candidate sensors were expressed in bacteria and the bacteria were subjected to the optimized bacterial lysis protocol. The lysates were screened for a lifetime change and a change in excitation and emission spectra, measured in both the calcium-bound and calcium-free states by addition of $CaCl_2$ or EDTA (Table 1, Figure S3).

Mutations T203Y and T203F both resulted in a red-shifted excitation and emission spectrum in both calcium states, but the shift was more pronounced for the T203Y mutation. This Tq-Ca-FLITS_T203Y variant also showed a large phase lifetime contrast of $\Delta\tau_\varphi$ = -0.9 ns. Surprisingly, this change is inverted compared to Tq-Ca-FLITS ($\Delta\tau_\varphi$ = 1.1 ns). The T203F mutation also inverted the lifetime response; however, the contrast was about half of the Tq-Ca-FLITS_T203Y variant. A mutation of I167F or I167H in the background of the T203Y variant,

or a separate I167F mutation on Tq-Ca-FLITS reduced the lifetime contrast and did not result in a (further) red shift.
We also tested the T203Y and T203H mutations on different circular permutations (cp) of Tq-Ca-FLITS, which we created in during the development of the turquoise sensor (van der Linden et al., 2021). In almost all cp variants with the T203Y mutation, the same red shift in both the excitation and emission spectra was observed as for Tq-Ca-FLITS_T203Y. An exception was the cp150-T203Y variant, where we observed a red shift only for the calcium-bound state in both excitation and emission spectra (Table S1, Figure S3). This variant differs from Tq-Ca-FLITS_T203Y by only a F146Y mutation. A T203H mutation did not cause a red shift in any of the cp variants.

Table 1. Lifetime and spectral screen of candidate sensors to create G-Ca-FLITS. Sensor variants are indicated by their mutations with respect to Tq-Ca-FLITS. The calcium-bound state (sat) is measured in presence of 0.1 mM $CaCl_2$ and the calcium-free state (apo) after addition of 9.5 mM EDTA.
*Emission and excitation maxima are only indicated if a red shift of the spectrum with respect to Tq-Ca-FLITS was observed. See also Figure S3.
**Phase lifetimes were measured at 37 °C by FD-FLIM. The lifetime change is calculated as the lifetime in the calcium-bound state minus the calcium-free state.

	Excitation max. (nm)*		Emission max. (nm)*		Phase lifetime (ns) **		
Sensor variant	**apo**	**sat**	**apo**	**sat**	**apo**	**sat**	**change**
Tq-Ca-FLITS	437, 455	437, 456	492, 502	480, 507	1.72	2.86	1.14
T203F	459	458	506	507	1.71	2.19	0.48
T203H	no red shift	no red shift	no red shift	no red shift	2.82	2.90	0.08
T203Y	461, 488	459, 478	516	514	3.08	2.20	-0.88
I167F, T203Y	460, shoulder 480	460, 479	512, shoulder 490	516	2.59	2.88	0.29
I167H, T203Y	459, 478	460, 479	514	519	2.92	3.11	0.18
I167F	no red shift	no red shift	no red shift	no red shift	1.52	2.17	0.65

Improving the green lifetime sensor by mutagenesis

We aimed to further improve Tq-Ca-FLITS_T203Y by mutagenesis in the regions linking the calcium binding domains to the FP. Using a PCR approach, we created a library of sensors with any possible amino acid on positions V27 and N271 (numbering according to the sensor). Bright green fluorescent colonies on an agar plate were selected for the bacterial lysis test. We found three sensors with an improved lifetime contrast: with alanine or valine on position 27, and aspartic acid or serine at position 271 (Table 2). The sensor with V27A and N271D gave the best results with a contrast of $\Delta\tau_\varphi$ = -1.4 ns. Notably, the lifetime contrast of Tq-Ca-FLITS_T203Y is larger than measured in the previous screen (Table 1), which is due to a difference in temperature: the first screen was performed at 37 °C while this second one was performed at room temperature.
Next, we measured the lifetime response of the three improved variants in HeLa cells (Table 2), before and after saturation of the sensor with ionomycin and calcium. Again, the variant with V27A and N271D gave the best results, with a lifetime change of -1.2 ns (both $\Delta\tau_\varphi$ and $\Delta\tau_M$, high calcium minus low calcium), which is an improvement of ~0.3 ns in lifetime change with respect to the parental sensor Tq-Ca-FLITs. We decided to name the new lifetime sensor G-Ca-FLITS, for **G**reen **Ca**lcium **F**luorescence **LI**fe**T**ime **S**ensor.

Table 2. Lifetime contrast of improved green versions of Tq-Ca-FLITS.
*'AD' stands for the mutations V27A and N271D, 'VS' for V27 and N271S, 'AS' for V27A and N271S.
**The fluorescence lifetime of bacterial lysates was measured at RT with by FD-FLIM after addition of 0.1 mM $CaCl_2$ and after addition of 9.5 mM EDTA. Mean phase lifetimes of the full field of view of the microscope are indicated.
***The fluorescence lifetime of HeLa cells expressing the different sensor variants was measured without stimulation and after addition of 5 µg/mL ionomycin and 5 mM calcium to the medium, measured at 37 °C. The mean and standard deviation (sd) of the fluorescence lifetime of all cells (n) are indicated.

		Bacterial lysate**		Response in HeLa cells***						
		Phase lifetime (ns)		Phase lifetime (ns)			Modulation lifetime (ns)			
Sensor variant*	**State**	**mean**	**change**	**mean**	**sd**	**change**	**mean**	**sd**	**change**	**n**
G-Ca-FLITS (Tq-Ca-FLITS_T203Y-AD)	apo	3.83	-1.37	3.19	0.08	-1.17	3.65	0.07	-1.15	314
	sat	2.45		2.02	0.06		2.50	0.08		267
Tq-Ca-FLITS_T203Y-VS	apo	3.39	-1.23	2.90	0.06	-0.92	3.37	0.07	-0.95	150
	sat	2.15		1.98	0.07		2.42	0.08		116
Tq-Ca-FLITS_T203Y-AS	apo	3.85	-1.23	3.19	0.08	-0.96	3.63	0.07	-0.89	306
	sat	2.62		2.23	0.06		2.74	0.06		345
Tq-Ca-FLITS_T203Y	apo	3.34	-1.13	2.95	0.08	-0.82	3.42	0.08	-0.85	193
	sat	2.21		2.13	0.06		2.57	0.07		201

Characterization of G-Ca-FLITS

In order to characterize its biophysical properties, we isolated G-Ca-FLITS from bacteria and purified the protein by a Ni-NTA column. The intermediate sensor Tq-Ca-FLITS_T203Y and a mTurquoise2 with T203Y mutation (mTq2_T203Y) were also purified for comparison (Table 3). G-Ca-FLITS shows excitation and emission spectra that are evidently red-shifted when compared to the Turquoise variant. The same is true for any of the versions that contain the T203Y mutation (Figure 1, Figure S4).

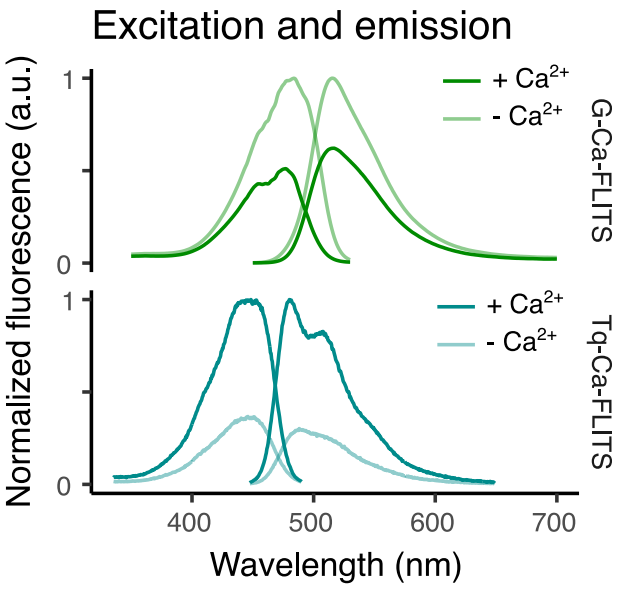

Figure 1. Excitation and emission spectra of G-Ca-FLITS and Tq-Ca-FLITS. The lighter lines indicate the calcium-free state (10 mM EGTA) and the darker lines the calcium-bound state (39 µM free Ca^{2+}). The Tq-Ca-FLITS is shown as a reference and was reported before (van der Linden et al., 2021). Spectra are normalized to the maximum of the calcium-free state for G-Ca-FLITS.

We determined the quantum yield (QY) of G-Ca-FLITS to be 41% for the calcium-free state, and 26% for the calcium-bound state (Table 3, Figure S5). This difference of 15% is slightly higher than in the intermediate variant Tq-Ca-FLITS_T203Y (13%). Interestingly, the quantum yield of mTq2_T203Y is 24%, comparable to the calcium-bound state of G-Ca-FLITS.
For G-Ca-FLITS, the extinction coefficient is for both states around 30,000 M^{-1} cm^{-1}, which is slightly higher than mTq2_T203Y (Table 3, Figure S6).

Table 3. Photophysical properties of G-Ca-FLITS and intermediate variant.
Apo – calcium-free state (10 mM EGTA), sat – calcium-bound state (39 µM free Ca^{2+}), ε - Extinction coefficient, QY – quantum yield with 95% confidence interval between curly brackets.

	state	λ_{abs} (nm)	λ_{em} (nm)	ε_{max} ($M^{-1}cm^{-1}$)	QY {CI} (%)
G-Ca-FLITS	apo	474	515	29300	41.1 {40.5 - 41.7}
	sat	476	517	30900	25.9 {25.4 - 26.5}
Tq-Ca-FLITS_T203Y	apo	470	516	28900	43.8 {43.2 - 44.3}
	sat	475	518	30900	30.7 {30.4 - 31.1}
mTq2_T203Y		471	514	27400	23.8 {23.5 - 24.2}

We measured the pH sensitivity of G-Ca-FLITS and mTq2_T203Y (Figure 2, Figure S7). In the calcium-free state the G-Ca-FLITS an increase in fluorescence lifetime in the range pH 4-6, followed by a stable lifetime above pH = 6. In contrast, in the calcium-bound state, the lifetime increases until pH = 5.5, followed by a drop and a stable lifetime above pH = 7. The mTq2_T203Y protein also shows a maximum of fluorescence lifetime at a low pH (pH = 4) followed by a drop and a stable lifetime above pH = 6.

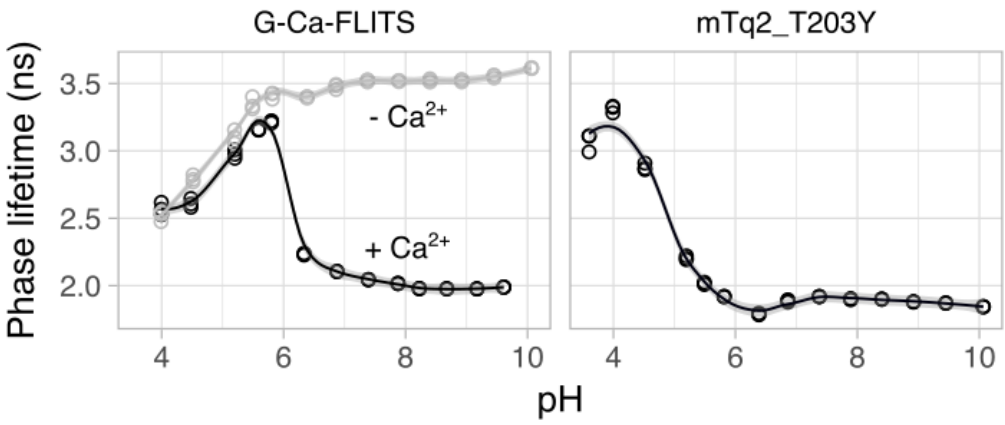

Figure 2. Influence of pH on phase lifetime of the proteins. Fluorescence lifetime of proteins diluted in pH buffer was measured (n=3). In case of G-Ca-FLITS, this was done in presence (gray, 0.1 mM $CaCl_2$) or absence of calcium (black, 5 mM EGTA). A smooth curve is fitted through the data using the loess method, using α = 0.4. The gray band indicates the 95% confidence interval of the smooth fit.

The calcium affinity of the lifetime readout of G-Ca-FLITS was determined at 37°C. To this end, we measured the lifetime of the sensor in a range of calcium buffers using Frequency-Domain FLIM (FD-FLIM) and plotted this in a polar space (Figure 3A, Figure S8). The two extreme values (zero calcium and 39 µM free calcium) are located on different coordinates in the polar plot and all intermediate concentrations are located on a straight line between these two

extremes. Based on the position in the polar plot, we determined the fraction of sensor in the calcium-bound state, while considering the intensity contribution of both states (Figure 3B).

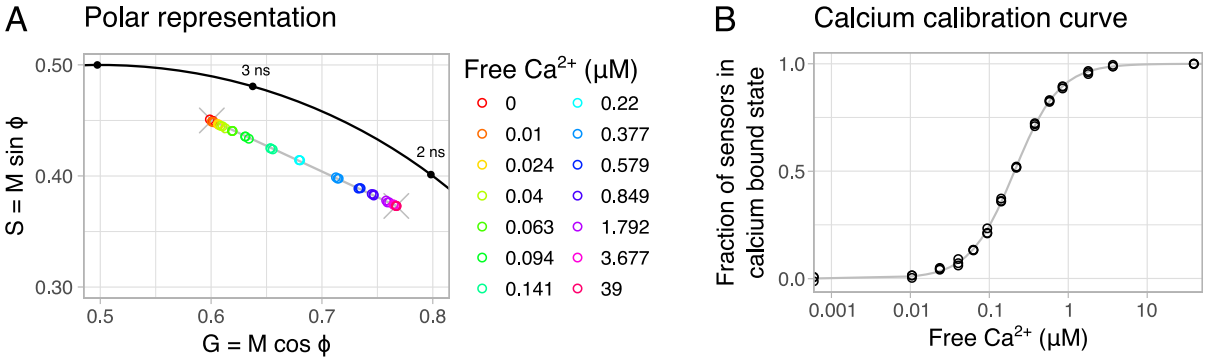

Figure 3. Calcium calibration of G-Ca-FLITS in vitro at 37°C. (**A**) The measured fluorescence lifetime of protein isolate of G-Ca-FLITS in a range of calcium concentrations is plotted in a polar space (n=3), with the color indicating the concentration. The measurements fall on a straight line (in gray) on the polar plot between the lowest and highest concentration (indicated by an X). (**B**) For each measurement, the fraction of sensors in the calcium-bound state (the low lifetime) is determined, taking the intensity contribution of the two extreme states into account. The fraction is plotted against the concentration of free calcium to obtain a calibration curve.

The intensity contribution was determined based on the excitation and emission spectra, the extinction coefficient per wavelength, the QY and the properties of the microscope, i.e. the excitation/emission filters, the excitation source and the detector sensitivity profile (Supplemental Note 1, Figure S9). A calibration curve was fitted to the fraction of sensors in the calcium-bound state for each concentration, from which the calcium affinity was determined to be K_D = 209 nM (Table 4). Using the variation in the measurements of the two extremes, we determined that we can reliably measure calcium concentration with G-Ca-FLITS at 37 °C between 14 nM and 16 µM. The same calibration was also performed at RT (Table 4, Figure S8). Here, the calcium affinity was K_D = 339 nM, higher compared to the calibration at 37°C. This is in line with the notion that binding strength generally increases with decreasing temperature.

Table 4. Calcium calibration parameters of G-Ca-FLITS. The calibration was performed with purified protein at two temperatures. The phase and modulation lifetime of the sensor are indicated for the two states of the sensor.
apo – in calcium-free buffer (10 mM EGTA), sat – in buffer with 39 mM free $CaCl_2$, τ_φ and τ_M – phase lifetime and modulation lifetime, K_D – calcium affinity with 95% confidence interval indicated between curly brackets, n – Hill coefficient with 95% confidence interval indicated between curly brackets.

Temperature	state	τ_φ (ns)	τ_M (ns)	K_D {CI} (nM)	n {CI}
37 °C	apo	2.98	3.50	209 {206-211}	1.53 {1.51-1.56}
	sat	1.93	2.43		
RT	apo	3.52	3.99	339 {335-343}	1.67 {1.64-1.70}
	sat	2.03	2.57		

Little change in intensity between the two states

During engineering and characterization of G-Ca-FLITS, we noted a low intensity contrast for the two extreme states. For a quantitative brightness analysis in cells, we co-expressed G-Ca-

FLITS and the red fluorescent protein mScarlet-I in HeLa cells from a single plasmid, using a P2A sequence (Kim et al., 2011; Liu et al., 2017).
We determined the ratio of green fluorescence over red fluorescence, to mitigate the effects of transfection efficiency, timing and cell thickness. The measurement was performed on both unstimulated cells, with a low intracellular calcium level, and cells stimulated with ionomycin and extra calcium to raise the calcium concentration to saturation of the sensor (Figure 4). To normalize the GFP/RFP ratio, we used EGFP-mScarlet-I and a construct without a green FP. G-Ca-FLITS and all its intermediate variants showed a higher intensity in both states compared to mTq2_T203Y. We measured a 0.70-fold change in GFP/RFP ratio for G-Ca-FLITS between the calcium saturated cells and the unstimulated cells.
To compare G-Ca-FLITS to other green GECIs, we repeated the experiment with G-GECO and several variants of GCaMP (Figure 4). In contrast to G-Ca-FLITS, these sensors show a high GFP/RFP ratio in the calcium saturated state and a low ratio in resting cells, resulting in a large ratio difference between the two states. The fold change was 5.6, 3.1, 4.6 and 6.3 for GCaMP3, GCaMP6s, jGCaMP7c and G-GECO1.1 respectively. The relative intensity of the GCaMPs/GECO in resting cells is much lower compared to the dimmest state of G-Ca-FLITS. We also found a larger standard variation in GFP/RFP in resting cells expressing GCaMP/G-GECO compared to G-Ca-FLITS.

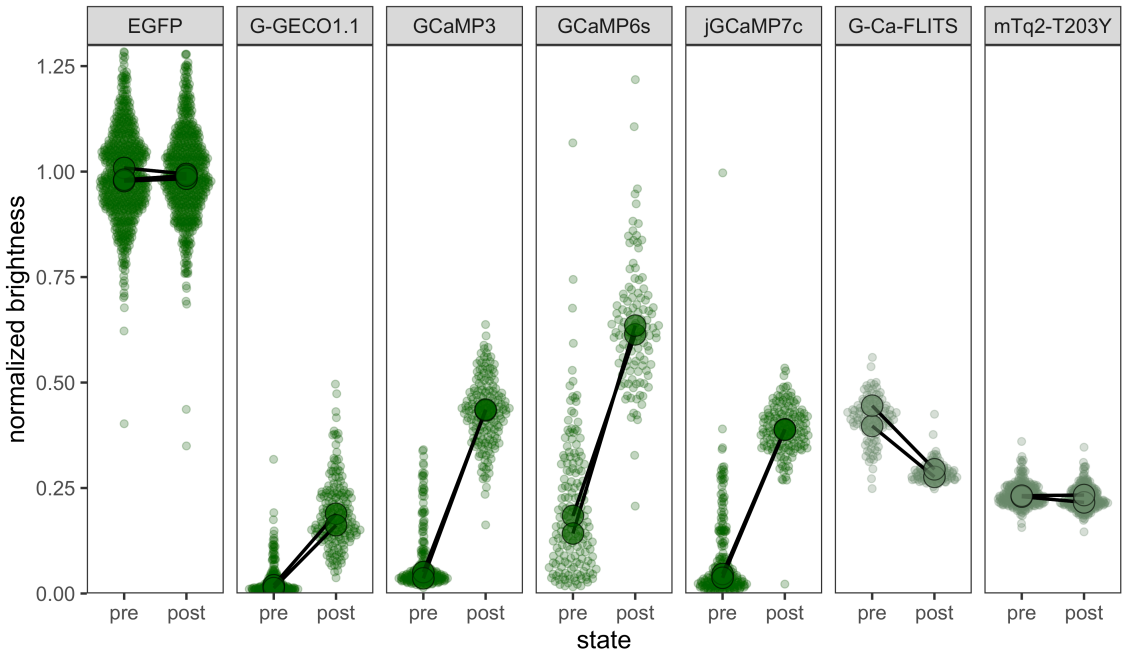

Figure 4. Brightness analysis of green fluorescent proteins and biosensors in HeLa cells using a co-expressed mScarlet-I. The ratio GFP/RFP was determined 24 h after transfection both in resting, unstimulated cells (pre) and cell stimulated with 5 µg/mL ionomycin and 5 mM calcium to reach saturation of the sensors (post). The ratios were normalized to cells expressing EGFP. Dots show individual cell data (n ≥ 99) and the large dot the average of each biological replicate (N = 2, except for EGFP; N=3).

The precision of the fluorescence lifetime depends on the number of photons. We hypothesized that the fluorescence lifetime of G-Ca-FLITS would have a similar precision in both low and high concentrations of calcium, given the small change in intensity. To examine this, we determined the signal to noise ratio (SNR = mean / standard deviation) of the fluorescence lifetime of G-Ca-FLITS in cells, measuring an area of 400 pixels (Figure 5, Figure

S10). Indeed, the SNR of G-Ca-FLITS is on average only 13% lower for the high calcium state. In comparison, the SNR of Tq-Ca-FLITS increases more than 2-fold when going from the low to high calcium state, in agreement with its 3-fold change in intensity. In all cases, the variation of the average lifetime of all cells is similar, meaning the average lifetime in the 400 pixels could be properly determined.

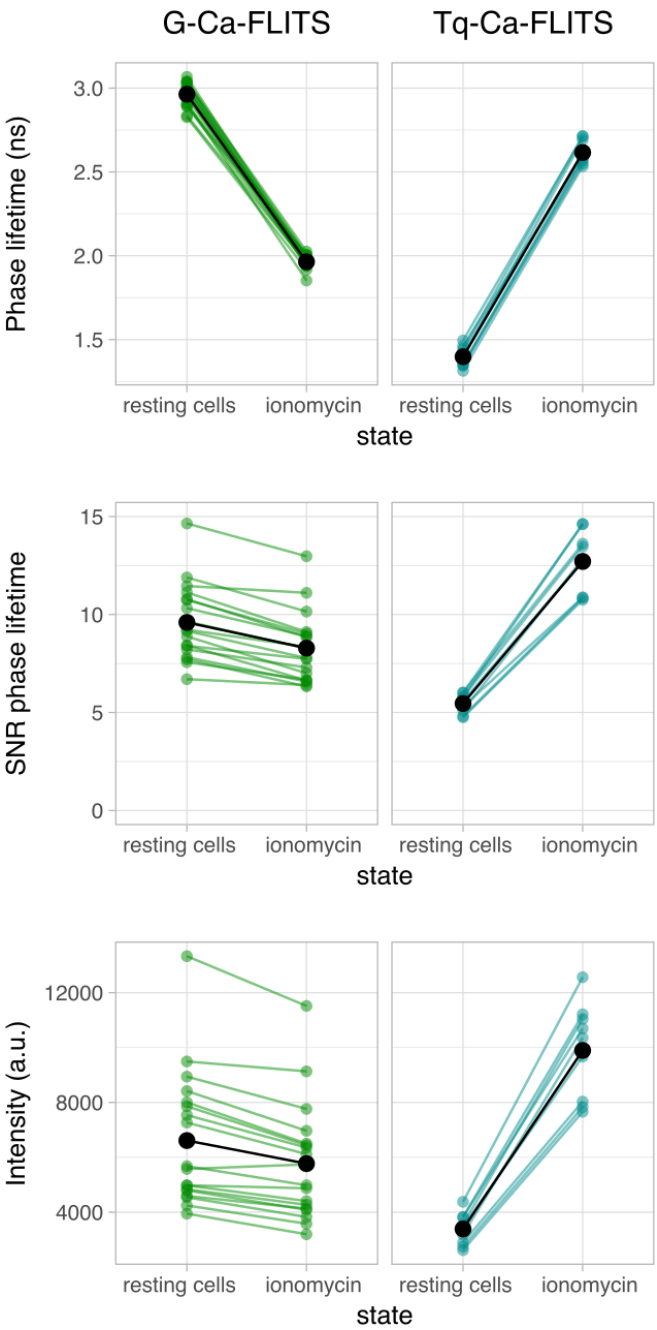

Figure 5. Comparison of the signal-to-noise ratio of the phase lifetime of G-Ca-FLITS and Tq-Ca-FLITS in HeLa cells. HeLa cells were measured in a resting state and after addition of 5 µg/mL ionomycin and 5 mM calcium. Measurements of individual cells are indicated by colored dots (n=18 for G-Ca-FLITS, n=9 for Tq-Ca-FLITS). Lines connect the measurements of the same cell. The average of all cells is shown in black. For each cell, 400 pixels were analyzed for the mean lifetime and intensity, and for the sd of the lifetime. SNR = mean lifetime / sd lifetime. Comparable phase lifetimes are found for all cells expressing a construct but the SNR is lower for lower intensity cells and varies less between the two states for G-Ca-FLITS.

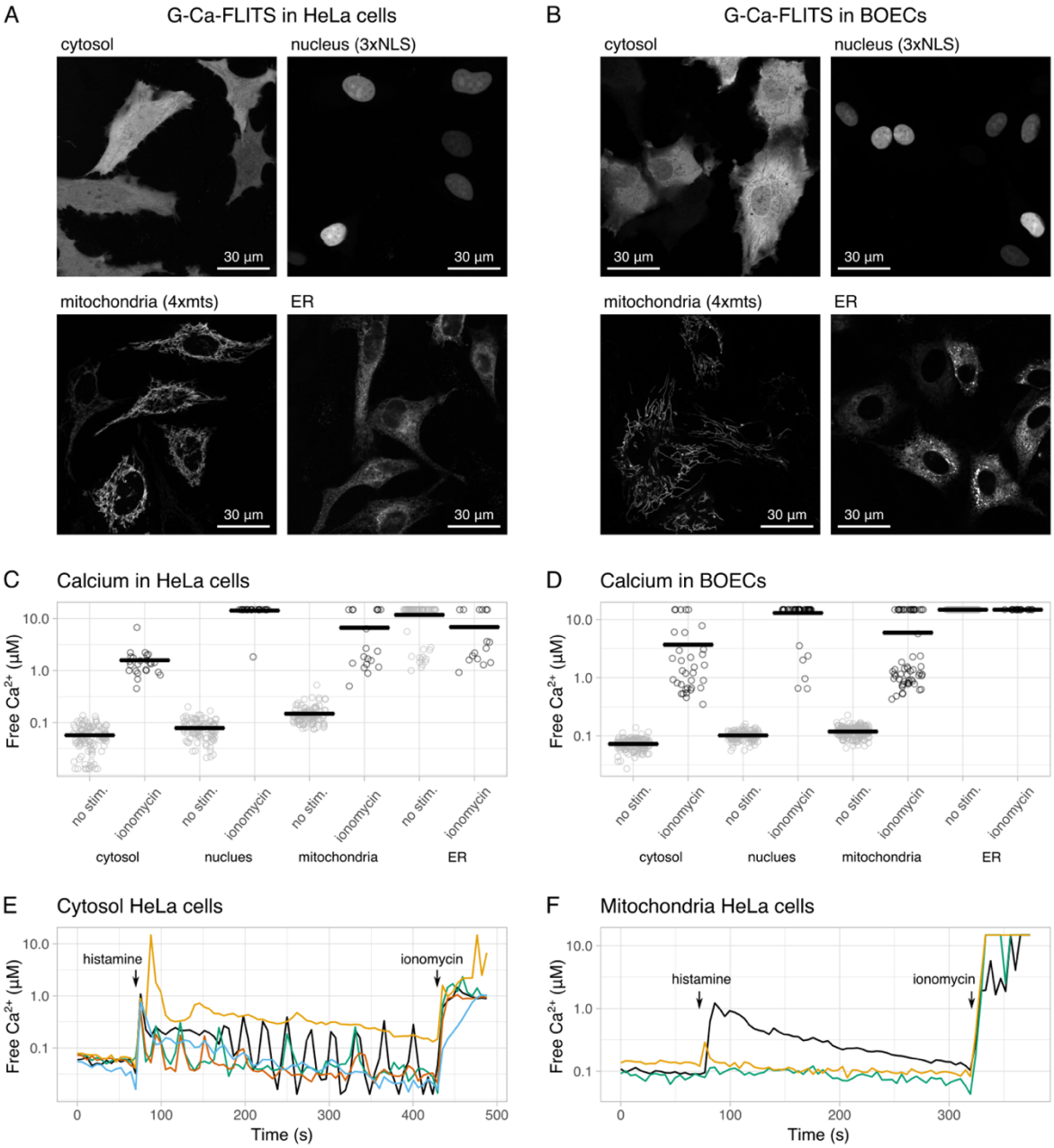

Figure 6. Measuring calcium concentrations in HeLa cells and BOECs using G-Ca-FLITS targeted to various organelles. (**A**) Localization of G-Ca-FLITS in HeLa cells and (**B**) in BOECs. Images are taken with a 63x magnification. (**C**) Measured calcium concentration in various organelles in HeLa cells and (**D**) BOECs. Measurements of single cells are indicated by circles, gray for unstimulated cells and black for cells after addition of 5 µg/mL ionomycin and 5 mM calcium. The mean of all cells is indicated by a black line. (**E**) Changing free calcium concentration after stimulation with 1 µM histamine or addition of 5 µg/mL ionomycin and 5 mM calcium in the cytosol and (**F**) in the mitochondria. Each line represents a single cell. Arrows indicate the moments of addition.

Measurement of calcium in organelles

Several tags were added to G-Ca-FLITS to target different organelles: the cytosol, the nucleus, the mitochondrial matrix, and the endoplasmic reticulum (ER). With the bright fluorescence of the probe independent of calcium, we could easily confirm the correct localization of the sensor to all targeted organelles, in both HeLa cells and Blood Outgrowth Endothelial Cells (BOECs) (Figure 6A, Figure 6B).

Next, we measured the calcium concentration in the various organelles in the same two cell types, using widefield FD-FLIM. Without stimulation, Hela cells showed an average calcium concentration of 57 nM in the cytosol, 79 nM in the nucleus and 148 nM in the mitochondria. After addition of 5 µg/mL ionomycin and 5 mM calcium, the average concentration was raised above 1 µM. In the ER the concentration was above 1 µM in all experiments. BOECs showed the same pattern, with average concentrations of 73 nM in the cytosol, 101 nM in the nucleus, 119 nM in the mitochondria and above 1 µM in the ER. After stimulation, the concentration in all organelles was elevated to above 1 µM (Figure 6C, Figure 6D).
In both cell types, no spatial differences were observed in unstimulated cells, except for the mitochondria of HeLa cells. Here, about 20% of the cells, had in peripheral parts a higher calcium concentration, comparable to the concentration in mitochondria after stimulation with ionomycin. These areas are not included in the calculations of the aforementioned averages.
HeLa cells expressing G-Ca-FLITS in the cytosol were stimulated with 1 µM histamine. We observed various patterns of oscillating calcium concentrations, confirming that binding of calcium to G-Ca-FLITS is reversible (Figure 6E). The calcium concentration was elevated to about 1 µM after addition of ionomycin and calcium, as seen before. The same experiment was repeated with HeLa cells expressing G-Ca-FLITS in the mitochondria (Figure 6F). Stimulation with histamine resulted in either no reaction or an elevation of the calcium concentration followed by a drop to basal level. Addition of ionomycin and calcium resulted in high concentrations as expected.

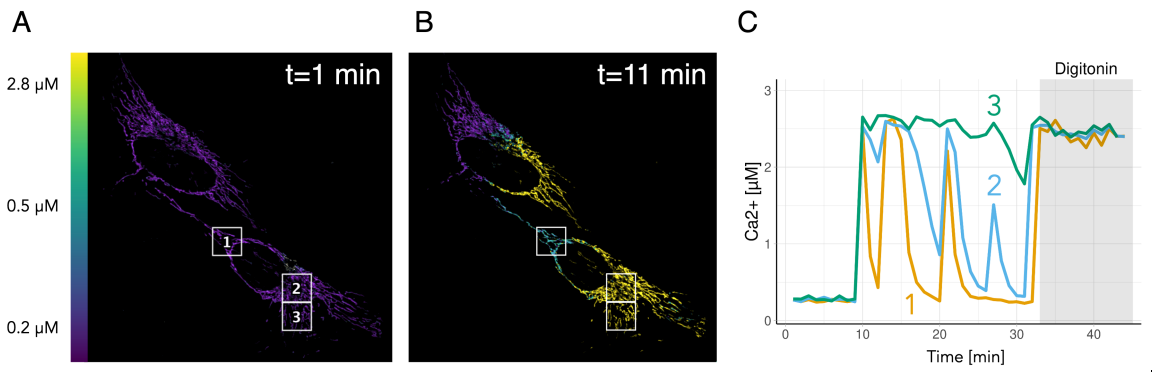

Figure 7. Quantitative imaging of spontaneous calcium dynamics in mitochondria. (A, B) FLIM images were acquired with a Leica Stellaris8 every 60 seconds and at the end of the sequence 10 µM digitonin was added to obtain a maximal response. The lifetime images were converted to calcium concentration using the K_D determined in vitro and the extremes from the lifetime image. False colors reflect the calcium concentration, according to the scale bar on the left. Calcium image at t=1 (A) and t=11 minutes (B), showing the three regions where calcium concentrations were quantified and displayed over time (C).

Since confocal imaging of fluorescence lifetime results in images with a better spatial resolution, we used a confocal microscope with a Time Correlated Single Photon Counting (TCSPC) detector to examine the heterogeneity that we observed in mitochondria. From the confocal lifetime images, it is evident that several cells have mitochondria that show a decreased lifetime in the periphery of the cell (supplemental figure 11). This indicates that mitochondria show heterogeneity and that a pool of mitochondria has increased calcium levels.

The confocal TCSPC system needs relatively long integration times (several minutes) and we turned to a Leica Stellaris system which allows for a >10-fold higher temporal resolution to study calcium dynamics. We introduced the 4mts-G-Ca-FLITS into HeLa cells and acquired a timelapse of lifetime images. At the end of the experiment digitonin was added to acquire the minimal lifetime, reflecting maximal calcium. Using the calibration curve that was generated using purified protein incubated with different calcium buffers (supplemental figure 12) we transformed the FLIM data into calcium concentration images as we did before. The calcium concentration images show the heterogeneity in calcium concentration and its dynamics over time (Figure 7). The elevated calcium concentrations are reversible but can last several minutes. Intriguingly, there is substantial difference in the dynamics between patches of mitochondria.

2P-FLIM

To assess the functionality of G-Ca-FLITS and Tq-Ca-FLITS with two-photon time-correlated single-photon counting (TCSPC) FLIM microscopy, we measured calcium in the brains of *Drosophila melanogaster* individuals affixed to a previously described stage (Maimon et al., 2010). Studies of activity-dependent transcription in neurons have used saline with elevated [K^+] to induce sustained and controlled increases in intracellular calcium. We employed a similar approach to raise external [K^+] from 3 mM to 103 mM by perfusing saline over the brain while imaging jGCaMP7f (Dana et al., 2019), Tq-Ca-FLITS and G-Ca-FLITS signals. Our experiments here focus on the EPG neurons, a population of neurons innervating the ellipsoid body region of the fly brain and which serve a role in navigation-related computations (Green et al., 2019; Seelig and Jayaraman, 2015) (Figure 8A).

jGCaMP7f exhibited large changes in fluorescence intensity several minutes after we elevated external [K^+] (Figure 8B). After a number of minutes (with the exact number varying from fly to fly), calcium levels fluctuated between low and high states synchronously across the field of view (including the EPG neurites visible in the middle of Figure 8D and the neurites of off-target cells in the bottom corners of the same images). The sample with jGCaMP7f showed only a very small change in lifetime in response to elevated calcium (0.030 nanoseconds ± 0.003, mean ±sd) despite the many-fold shift in fluorescence intensity (5.79 $\Delta F/F$ ± 0.503 (mean ± sd).

Tq-Ca-FLITS fluorescence was higher than that of jGCaMP7f at baseline (Figure 8D). In contrast, despite the high brightness of G-Ca-FLITS in the apo state in other systems, the baseline intensity of G-Ca-FLITS in these fly neurons was much lower than both jGCaMP7f and Tq-Ca-FLITS, for unclear reasons. Even with increased laser power, G-Ca-FLITS was dimmer than jGCaMP7f at baseline (see Methods) (Figure 8D, top row). In response to elevated [K^+], Tq-Ca-FLITS showed large increases in fluorescence (1.672 $\Delta F/F$ ± 0.299, mean ± sd) and empirical lifetime (0.893 nanoseconds ± 0.043, mean ± sd) (Figure 8D). The response of G-Ca-FLITS was also consistent with increases in intracellular calcium: this sensor exhibited large decreases in empirical lifetime (-0.465 nanoseconds ± 0.101 (mean ± sd)) (Figure 8C), and a modest decrease in intensity (-0.339 $\Delta F/F$ ± 0.043, mean ± sd) after perfusion of elevated external [K^+] (Figure 8B, 8E). The lifetime response of Tq-Ca-FLITS and the $\Delta F/F$ response of jGCaMP7f resembled each other, with both signals gradually increasing over the span of 3-4 minutes after we increased external [K^+]; the two signals then hit a plateau for ~1 min, followed by a return to baseline and often additional plateaus (Figure 8B-C). By comparison, G-Ca-FLITS responses were more variable, typically exhibiting a smaller ramping phase and seconds-long spikes of activity rather than minutes-long plateaus (Figure 8C).

Overall, all three fluorophores exhibit calcium-dependent signals in an intact brain using 2P-FLIM. The Tq-Ca-FLITS lifetime response is particularly large and shows much higher brightness under 2P excitation than G-Ca-FLITS in both the baseline and high calcium states.

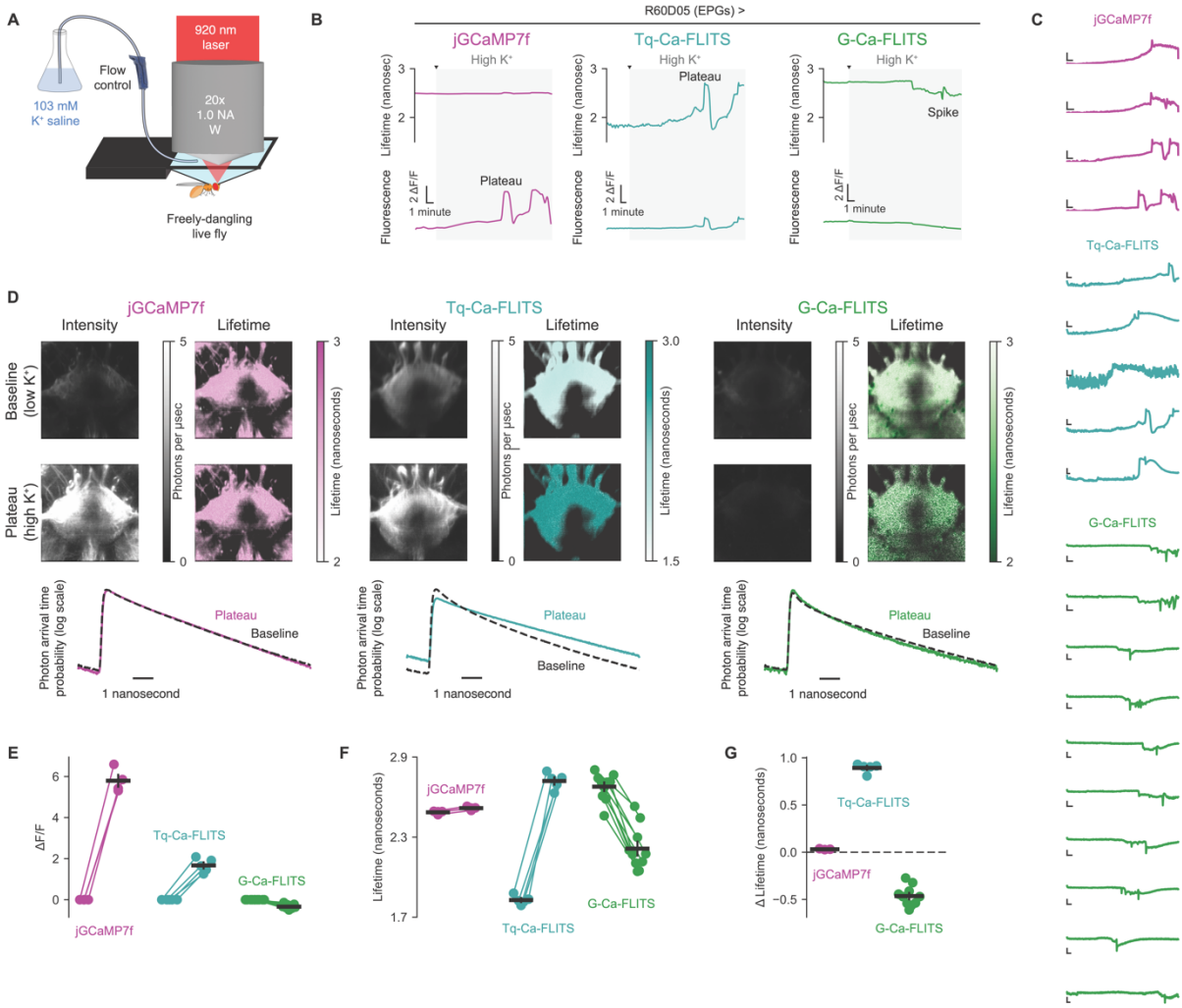

Figure 8. Two-photon TCSPC signals from G-Ca-FLITS and Tq-Ca-FLITS, and comparison to jGCAMP7f, in an intact Drosophila brain.

(**A**) Schematic of a head-fixed live *Drosophila melanogaster* female, imaged with standard saline for two minutes before perfusing a high [K^+] saline variant over the brain.

(**B**) Single example traces of flies expressing jGCaMP7f (pink, left), Tq-Ca-FLITS (turquoise, center) or G-Ca-FLITS (green, right) in the EPG neurons under the control of R60D05-Gal4. Top row: Tq-Ca-FLITS and G-Ca-FLITS show strong FLIM changes in response to elevated [K^+] while jGCaMP7f shows very little. Bottom row: jGCaMP7f and Tq-Ca-FLITS exhibit large changes in fluorescence while G-Ca-FLITS becomes moderately dimmer. Gray region indicates time when high K+ saline was perfused.

(**C**) Intensity traces from all flies. Vertical scalebars: 0.200 nanoseconds for G-Ca-FLITS and Tq-Ca-FLITS, 5 ΔF/F for jGCaMP7f. Horizontal scalebars: 1 minute.

(**D**) Fluorescence (left) and FLIM (right) images of example flies from panel B before [K^+] elevation (baseline, 2 minute average, top row) and for the 30 second surrounding the peak change in calcium (second row). Lifetime images are masked to show only automatically-determined "foreground" pixels. Third row: photon arrival time histograms for the data of the above rows.

(**E**-**G**) Summary statistics for all flies (from panel **C**). (**E**) shows changes in fluorescence intensity, (**F**) shows absolute lifetime measurements, and (**G**) reflects the change in lifetime from baseline to plateau for each of the three indicators.

DISCUSSION

Most fluorescent biosensors toggle between a dim and a bright state. The dim fluorescence decreases the SNR, thereby increasing the measurement error in quantitative imaging. Here, we present a green calcium biosensor, G-Ca-FLITS, that maintains a consistent brightness over its full dynamic range. The calcium-dependent lifetime decrease of 1.2 ns when calcium is elevated can be used to quantify calcium concentrations in cells. In comparison, the cyan/turquoise sensor Tq-Ca-FLITS we previously developed (van der Linden et al., 2021) shows a 3-fold change in intensity combined with a similar change in lifetime. The intensity of G-Ca-FLITS is higher than the dim (calcium-free) state of several popular green GCaMPs, and comparable to the bright state of most tested sensors, as determined by ratio imaging with co-expression of mScarlet-I. Of the tested GCaMPs, GCaMP6s seems to have a fairly bright calcium-free state, and we believe this is due to the higher calcium affinity (K_D = 144 nM) of this sensor (Chen et al., 2013). In contrast, the affinities are 339 nM, 298 nM and 618 nM at room temperature, for G-Ca-FLITS, jGCaMP7c (Dana et al., 2019) and G-GECO1.1 (Zhao et al., 2011), respectively.

The minimal change in fluorescence intensity compared to other commonly used calcium biosensors results in a similar SNR for both states of G-Ca-FLITS. Therefore, low concentrations of calcium can be precisely measured in unstimulated mammalian cells, as well as increased concentration after stimulation. The quantitative measurements require calibration of the biosensor response to different calcium concentrations. Although the calibration is equipment independent under ideal conditions, and only needs to be performed once, we prefer to repeat the calibration for different set-ups to account for differences in temperature or pulse frequency.

Our measured concentrations in resting cells agree with literature, 20 - 100 nM is reported for cytoplasm and nucleus, and a slightly higher concentration of 50 - 300 nM in the mitochondria (Arnaudeau et al., 2001; Berridge et al., 2000; Dalal et al., 2020; Palmer et al., 2006; Rotrosen and Gallin, 1986; Worthen and Nollert, 2000). Free calcium in the ER is reported to be >300 µM, well above saturation of G-Ca-FLITS (Arnaudeau et al., 2001). Another advantage of a consistently bright probe is that cells and structures labeled with the biosensor can be readily visualized.

Using G-Ca-FLITS, we were able to detect various (oscillating) patterns of calcium in HeLa cells after stimulation with histamine. These data show that the sensor is suitable for detection of repeated transient calcium elevations. Importantly, G-Ca-FLITS gives a stable read-out at the high pH of 8.0 in mitochondria. We observed high calcium level in some peripheral mitochondria in HeLa cells, but not in endothelial cells. Others have shown heterogenous responses of calcium (Greotti et al., 2019; Palmer et al., 2006) and electrical signals (Collins et al., 2002) in mitochondria. However, this is different from the sustained high levels we observed in exclusively peripheral parts of the cells, without any stimulation. Studies show that mitochondria can be distinguished in different pools based on their location and function (Ngo et al., 2021; Park et al., 2001). Peripheral mitochondria are one of these groups and have less connections to the ER compared to other pools. These connections play an important role in calcium signaling of the mitochondria (Giorgi et al., 2018). In cancerous cells, like HeLa cells, the mitochondrial calcium homeostasis can be dysregulated (Delierneux et al., 2020). We speculate that this leads to the sustained high levels of calcium in some peripheral mitochondria, possibly linked to aberrant connections to the ER.

To our knowledge, the sustained high levels we observed in mitochondria have not been reported yet. The types of probes used so far might be a contributing factor. Detecting the sustained high levels without stimulation is hardly possible with a probe that only shows an intensity response, like the widely used Rhod-2 or Aequorin. It is possible by using filterFRET/sensitized emission (Gadella, 2009), but this requires extensive controls. Also, much research in mitochondria has been focused on the rise in calcium after stimulation, and therefore probes with a high K_D (over 1 µM) have been used preferably (Arnaudeau et al., 2001; Fernandez-Sanz et al., 2019; Fonteriz et al., 2010; Palmer et al., 2006). This low affinity might be too low to detect the effect we have seen.

G-Ca-FLITS shares its > 1 ns lifetime contrast and pH stability with the cyan/turquoise sensor Tq-Ca-FLITS we previously developed (van der Linden et al., 2021), but the green emission is advantageous for several reasons: 1) excitation for green FPs is installed on virtually every lifetime microscope, while excitation for cyan FPs is less common, 2) the phototoxicity will be less and the penetration depth will be improved, and 3) it provides possibilities for multiplexing with Förster Resonance Energy Transfer (FRET)-FLIM sensors that often harbor a cyan-yellow FP pair, for example EPAC (Klarenbeek et al., 2015).
A recent effort to generate a green emitting lifetime biosensor used a GFP variant as a template (Koveal et al., 2022), and the resulting biosensor was pH sensitive in the physiological range. On the other hand, biosensors with a CFP-like chromophore are largely pH insensitive (van der Linden et al., 2021; Zhong et al., 2024). Therefore, we expect that a circular permuted fluorescent protein with a CFP chromophore and the T203Y mutation is a good template to generate pH-insensitive green lifetime-based sensors

The unique properties of the new green calcium sensor are evident from its photophysical properties. The extinction coefficient of the calcium-bound and -free states of G-Ca-FLITS is very similar, but the difference in QY is significant. Interestingly, the lower QY is observed in the calcium-bound state and is very similar to the QY of mTq2_T203Y, the FP that is used in this probe. This, combined with the resemblance in spectral shape and pH sensitivity, indicates that in the calcium-bound state the FP-barrel is probably in roughly the same closed conformation as mTq2_T203Y. When calcium is removed, a more open state is assumed with a more favorable QY, linked to a higher lifetime. Usually, a higher QY results in a higher intensity; however, in G-Ca-FLITS the open state has a differential shaped excitation spectrum which leads to a decreased intensity. These effects combined have resulted in a sensor where the two different states have a similar intensity despite displaying a large QY and lifetime contrast. Possibly, the lifetime contrast could be further improved by increasing the QY of the calcium-free state; however, it remains uncertain which effect that might have on the (lack of) intensity change.

We evaluated the use of Tq-Ca-FLITS and G-Ca-FLITS for 2P-FLIM and observed a surprisingly low brightness of the green variant in an intact fly brain. This result is consistent with a study finding that red-shifted fluorescent-protein variants that are much brighter under one-photon excitation are, surprisingly, dimmer than their blue cousins in multi-photon microscopy (Molina et al., 2017). The responses of both probes were in line with their properties in single photon FLIM, but given the low brightness of G-Ca-FLITS under 2-photon excitation, the Tq-Ca-FLITS may be a better choice for 2P-FLIM experiments.

In conclusion, we developed a green fluorescent GECI, named G-Ca-FLITS, with a lifetime contrast of over 1 ns, and a modest intensity change. This sensor does not have one (very) dim state unlike other green GECIs, therefore the variation in the measurement is comparable in both states. In addition, the lifetime response is stable above pH 7. We successfully measured the calcium concentration in various organelles in both HeLa cells and BOECs, including the mitochondria. A portion of HeLa cells show sustained high levels of calcium in some peripheral mitochondria, but further research is required to determine the origin of this heterogeneity. We anticipate that the G-Ca-FLITS will be a valuable tool to examine the heterogeneity of calcium concentrations in mitochondria and other cellular compartments.

METHODS

General Cloning. We used *E. coli* strain *E. cloni* 5-alpha (short: *E. cloni*, Lucigen corporation) for all cloning procedures. For DNA assembly, competent *E. cloni* was transformed using a heat shock protocol according to manufacturers' instructions. For protein expression, *E. cloni* was grown using super optimal broth (SOB, 0.5% (w/v) yeast extract, 2% (w/v) tryptone, 10 mM NaCl, 20 mM $MgSO_4$, 2.5 mM KCl) supplemented with 100 µg/mL kanamycin and 0.2% (w/v) rhamnose (SKR). For agar plates, 1.5% (w/v) agar was added. Bacteria were grown overnight at 37 °C. Plasmid DNA was extracted from bacteria using the GeneJET Plasmid Miniprep Kit (Thermo Fisher Scientific) and the obtained concentration was determined by Nanodrop (Life Technologies).
DNA fragments were generated by PCR, using Pfu DNA polymerase (Agilent Technologies) unless otherwise indicated. DNA fragments were visualized by gel electrophoresis on a 1% agarose gel, run for 30 min at 80 V. PCR fragments were purified using the GeneJET PCR purification Kit (Thermo Fisher Scientific) and digested with restriction enzymes to generate sticky ends. Restriction enzymes were heat inactivated at 80 °C for 20 min if necessary. Vector fragments were generated by restriction of plasmids and the correct bands were extracted from gel using the GeneJET Gel Extraction Kit (Thermo Fisher Scientific). DNA fragments were ligated using T4 DNA ligase (Thermo Fisher Scientific), per the manufacturers' protocol.
For targeted mutagenesis, we used the protocol as described before (Bindels et al., 2014). Primers were designed with an annealing region of 15 bp both left and right of the desired mutation(s). The full plasmid was amplified by PCR and the DNA was digested with DpnI to remove template DNA. *E. cloni* was transformed with the digested PCR mix and individual colonies were selected for isolation of individual colonies.
Correct construction of plasmids was verified by control digestion and sequencing (Macrogen Europe). All primers (Table S2) were ordered from Integrated DNA Technologies.

Engineering of G-Ca-FLITS. Tq-Ca-FLITS was subjected to mutagenesis of residues T203 and I167 (both mq2 numbering), by cloning using in vitro assembly, IVA (García-Nafría et al., 2016). First, full plasmids were replicated by PCR while introducing the desired mutation using the dual expression plasmid pFHL-Tq-Ca-FLITS (Addgene plasmid #129628) as template, primers 1-2, 3-4 or 5-6 and Phusion DNA polymerase (Thermo Fisher Scientific). The resulting PCR mix was DpnI digested and 4 µl of the mix was used for transformation of *E. cloni*. The linear DNA fragments were assembled into a plasmid in bacteria using a 15 bp homologous region at the ends of the fragments. In addition, intermediate, differently circular permutated variants of Tq-Ca-FLITS were subjected to mutagenesis of T203 by using primers 1-2 and the IVA method described above. Individual colonies were picked for testing of the excitation and emission spectra, for testing of the lifetime response and for plasmid isolation and sequencing.
The best performing variant was subjected to further mutagenesis of the sequences linking the FP with the CaM and M13 peptide. A library of variants was created by PCR with pFHL-Tq-Ca-FLITS as template and primers 7-8. The PCR fragments and a pFHL backbone (containing R-GECO1, a red calcium sensor) were digested using SacI and MluI, followed by ligation. Individual colonies were picked for screening of the excitation and emission spectra and of the lifetime response. Plasmids of interesting variants were isolated for sequencing.

Generation of the dual expression vector for ratiometric measurements.
The SacI restriction site was removed from mScarlet-I in an 'empty' pDress plasmid (Bindels et al., 2020), containing mScarlet-I linked to an anti-FRET linker and a P2A site (Addgene plasmid #130509, but with the mScarlet protein between the AgeI and BsrGI sites replaced with the DNA sequence GCCTCAACATGA and mTurquoise2 replaced by mScarlet-I). The SacI site was removed by directed mutagenesis using primers 9-10, see '**General cloning'**. After mutagenesis, correct removal of the SacI site and the absence of unwanted spontaneous mutations was verified by control digestion with SacI and NheI followed by sequencing. This yielded pDress_mScI_antiFRET_P2A_linker-noSacI (internal number 5517).
An insert fragment was amplified from the new plasmid by PCR using primers 11-12, containing the last part of the rhamnose promotor, the ribosome biding site, the adapted kozak sequence, the 6xHis-tag, the thrombin recognition site, the mScarlet-I fluorescent protein, the anti-FRET linker and the P2A sequence. A PCR using Phusion polymerase (Thermo Fisher Scientific) was performed on dual expression plasmid pFHL (Addgene plasmid #129628) using primers 13-14 to generate a backbone fragment containing the Tq-Ca-FLITS calcium sensor, the backbone of the pFHL plasmid, the CMV promotor and the first part of the rhamnose promotor. Both insert and backbone fragment were digested with BamHI and EcoRI to create overhanging ends. The fragments were ligated together and *E. cloni* was transformed with the DNA. We named this plasmid pFR_mScarletI-antiFRET-P2A-mTurquoise2_T203Y. Correct construction of the new pFR (Franka Ratio) plasmid was verified by control digestion with NheI and BsrGI and sequencing.
G-Ca-FLITS and intermediate variants were put in the ratioplasmid pFR by restriction (MluI and SacI) and ligation of pFR_mScarletI-antiFRET-P2A-mTurquoise2_T203Y and a pFHL plasmid containing the sensor of interest. Correct insertion was verified by sequencing.
As control, also EGFP and green variants of mTq2 and sfmTq2 were put in the pFR plasmid. The FPs mTq2 and sfmTq2 were subjected to directed mutagenesis to create mTq2_T203Y and sfmTq2_T203Y with primers 15-16. Next, PCR fragments were created of the green turquoise FPs and EGFP by using primers 17-18. PCR fragments and a pFR backbone were digested with BamHI and HindIII, followed by ligation. Correct insertion was verified by sequencing.
Green GECIs were put in pFR for comparison. DNA fragments were created by PCR using pGD-CMV-jGCaMP7c (Addgene plasmid #105320), pcDNA3-Cyto-GCaMP3 (Addgene plasmid #64853), pGP-CMV-GCaMP6s (Addgene plasmid #40753) and CMV-G-GECO1.1 (Addgene plasmid #32445) as template and primers 19-20. The fragments and a pFR backbone were digested with BamHI and HindIII, and ligated together. Correct insertion was verified by sequencing.

Plasmids for expression in organelles. The sensor sequence was amplified by PCR to generate cytoplasmic, nuclear, mitochondrial and ER-targeted versions of G-Ca-FLITS for transient transfection of mammalian cells, using primers 21-22 (for ER) or 21 and 23 (all others). DNA fragments and vectors carrying the desired tag were digested with AgeI and BsrGI, followed by ligation. Of the following vectors the FP was exchanged for Tq-Ca-FLITS: 3xnls-mTurquoise2 (Addgene plasmid #98817) for a nuclear tag, 4xmts-mScarlet-I (Addgene plasmid #98818), ER-mScarletI (Addgene plasmid #137805) and mVenus-N1 (color variant of Addgene plasmid #54843) for an untagged version.

Screening of sensors in bacterial lysate. *E. cloni* bacteria were used for screening of green calcium sensor variants. Bacteria expressing (a library of) sensor variants on pFHL plasmids were grown on SKR-agar plates. Colonies visually showing a (bright) green fluorescence (excitation filter 470/40 nm, emission filter 525/50 nm) under a stereomicroscope (MZFLIII, Leica) were selected. Bacteria were grown overnight in 1.5 mL SKR in a deep well plate (732-2893, VWR) covered with an adhesive seal (AB-0718, Thermo Fisher Scientific) at 37 °C while shaking at 280 rpm. The next day, 1 µL of culture was spotted on a SKR plate for storage, and the remainder of the bacteria were harvested by 15 min centrifugation at 2683 ×g in a swing-out centrifuge (5810 R, Eppendorf). Supernatant was removed and 200 µL of lysis buffer (2% Deoxycholic acid in 50 mM Tris-HCl pH 8.0) was added. During optimization of the lysis protocol, the lysis buffer consisted of 50 mM Tris-HCl pH 8.0 with DOC (0, 1, 2 or 3%), urea (0, 0.5 or 1 M), lysozyme (1 mg/mL), Sodium dodecyl sulfate (0, 0.1, 0.25 or 0.5%) and/or Triton-X100 (0, 0.1, 0.5 or 1%). Bacteria were brought in suspension using a vortex and incubated for 15 minutes at RT while intermittently shaking. If indicated, the plate with suspensions was frozen at -20 °C and thawed. Cell debris was removed by 40 min centrifugation at 2683 ×g in a swing-out centrifuge. The bacterial lysate was collected and stored overnight at 4 °C. The next day, bacterial lysates were diluted 2.5-4×, in 50mM Tris-HCl pH 8.0 to a final volume of 200 µL in 96-well plates with black walls and a glass bottom (89626, Ibidi).
A JASCO FP-8500 spectrofluorometer with microplate reader adapter was used to measure the excitation and emission spectra. Excitation spectra were measured at 370 - 490 nm with a 2.5 nm bandwidth and 1 nm intervals, while collecting emission at 530 nm with 10 nm bandwidth, using a scan speed of 1000 nm/min, 50 ms response time and a high sensitivity. Emission spectra were measured at 460 - 600 nm with a 2.5 nm bandwidth and 1 nm intervals, while exciting at 425 nm with 5 nm bandwidth, using a scan speed of 1000 nm/min, 0.1 s response time and a high sensitivity. Each spectrum was correct for background by subtraction of the spectrum of a well with only buffer. The same plate was used for determination of the fluorescence lifetime of the lysates as described under '**Lifetime imaging.'** Spectra and lifetimes were recorded after addition of 0.1 mM $CaCl_2$ (10 µl of 2 mM) to saturate the sensors, and again in the same wells after addition of 9.5 mM EDTA (10 µl of 0.2 M) to remove all calcium from the sensors. After analysis, interesting colonies were picked and grown for further investigation from the agar plates with spotted colonies.

HeLa cell culture and transfection. HeLa cells (CCL-2) acquired from the American Tissue Culture Collection were maintained in full medium, Dulbecco's modified Eagle medium + GlutaMAX (61965, Gibco) supplemented with 10% fetal bovine serum (FBS, 10270, Gibco), under 7% humidified CO_2 atmosphere at 37 °C. Cells were washed with Hank's buffered salt solution (HBSS, 14175, Gibco) and trypsinized (25300, Gibco) for passaging. No antibiotics were used.
HeLa cells were grown in 24-well plates with a glass bottom for imaging (Thermo Fisher Scientific). Transfection mixture was prepared in Opti-MEM (31985047, Thermo Fisher Scientific) with 2 µg Polyethylenimine in water (PEI, pH 7.3, 23966, Polysciences), 50 ng plasmid DNA and 150 ng mock-DNA (empty plasmid), and incubated for 20 min before addition to the cells. Cells were imaged 1- or 2-days post-transfection. Before imaging, the medium was replaced with microscopy medium (137 mM NaCl, 5.4 mM KCl, 1.8 mM $CaCl_2$, 0.8 mM $MgSO_4$, 20 mM D-Glucose, 20 mM HEPES pH 7.4) and cells were incubated for 20 min.

BOEC cell culture and microporation. Cord blood Blood Outgrowth Endothelial cells (cbBOEC) were cultivated from healthy donor umbilical cord blood as described before (Martin-Ramirez et al., 2012). Cells were cultured in Endothelial Cell Growth Medium-2 BulletKit (CC-3162, Lonza) supplemented with 100 U/mL Penicillin (Thermo Fisher Scientific) and 100 µg/mL Streptomycin (Thermo Fisher Scientific) and 20% FBS, under 5% humidified CO_2 atmosphere at 37 °C. cbBOECs were cultured from passage number 4 to 16. Culture dishes and microscopy plates were coated with 0.1% gelatin (Merck) in phosphate-buffered saline 30 min prior to cell seeding.
Cells were transfected by microporation with 2 µg plasmid DNA containing G-Ca-FLITS tagged to various organelles per 3-5 x 10^5 cells. For microporation, the Neon Transfection System (MPK5000, Invitrogen) and corresponding Neon transfection kit were used according to manufacturers' protocol. We used the R buffer from the kit, the 100 µL tips, and a 30 ms pulse of 1300 V. After microporation, BOECs were directly seeded in 24-well plates with a glass bottom (Thermo Fisher Scientific). After two hours, the medium was replaced. Cells were imaged 24 h after transfection in full medium.

Frequency domain Lifetime imaging. For FD-FLIM lifetime measurements, we used a Lambert Instruments FLIM Attachment (LIFA) setup, composed of an Eclipse Ti microscope (Nikon) with a Lambert Instruments Multi-LED for excitation, a LI^2CAM camera, a LIFA signal generator (all Lambert Instruments) to synchronize the light source and the camera, and was controlled by the LI-FLIM software (version 1.2.13). For GFP measurements, a 446 nm light emitting diode (LED) was used, combined with a 448/20 nm or 472/30 nm excitation filter, a 488 nm dichroic mirror and a 520/35 nm band-pass filter. For CFP measurements, a 446 nm LED was used, combined with a 448/20 nm excitation filter, a 442 nm dichroic mirror and a 482/25 nm band-pass filter (all filters from Semrock). The LED and image intensifier were high-frequency modulated at 40 MHz. Alexa488 or EB was used as a reference to calibrate the instrumentation, with a known mono-exponential lifetime of 4.05 ns (Rusinova et al., 2002; Zheng et al., 2018) or 0.086 ns (Bastiaens et al., 1992; Boens et al., 2007; van Munster and Gadella, 2004), respectively.
Fluorescence lifetime of sensors in bacterial lysates was recorded at RT or 37 °C using a ×20 (Plan Apo, NA 0.95 air) objective or a ×40 (Plan Apo, NA 0.95 air) objective, collecting 12 phase images and averaging 3×. When measuring lysates in a 96 well-plate, the LIFA software was controlled by a Matlab script (Bindels et al., 2014) that automatically moves to the position of each of the wells, adjusts the exposure time based on the intensity to a maximum of 500 ms, collects the lifetime stack and saves the data. Fluorescence lifetime in HeLa cells or BOECs was recorded at 37 °C. If needed, 1 µM histamine or a mix of ionomycin (5 µg/mL, I-6800, LClaboratories) and calcium (5 mM) was added. Cells were imaged using a ×40 (Plan Apo, NA 0.95 air) objective and collecting 12 phase images.
Recorded sample stacks and a reference stack were converted into lifetime images by an ImageJ macro (Bindels et al., 2020; Gadella et al., 1994). When the intensity of fluorescence in the cells was very weak, a background correction was performed on the lifetime stacks, using a manually indicated background region using Matlab (R2015a). For bacterial lysates, the average phase and modulation lifetime (τ_ϕ and τ_M) of the full view were extracted by the imageJ macro described above. For cells, the lifetime of individual cells with was collected. This was done in a semi-automatic manner, using first an ImageJ macro that masks the image based on intensity, followed by a macro that guides the measurements of the cells and the saving of the ROIs. For signal-to-noise calculations, a rectangular ROI was drawn manually

inside cells with an area of 400 pixels (20×20, 10×40 or 5×75 pixels), from which the mean and standard deviation were extracted.

Protein isolation. Plasmid were prepared for isolation of the proteins mTq2_T203Y, G-Ca-FLITS and intermediate variant Tq-Ca-FLITS_T203Y. To this end, mScarlet-I, the anti-FRET linker and the P2A site were removed from the pFR plasmids containing the proteins of interest by digestion with NheI followed by ligation. The new plasmids were named pFPO-mTq2_T203Y, pFPO-G-Ca-FLITS and pFPO-Tq-Ca-FLITS_T203Y (FPO being an abbreviation for Franka Protein Only) and correct removal was verified by sequencing.
E. cloni bacteria containing a pFPO plasmid were grown overnight in 50 mL SKR medium at 37 °C while shaking. The next morning, the cultures were put at 20 °C for 6 hours, while shaking. Bacteria were harvested by centrifugation for 30 min at 3220 ×g (5810 R, Eppendorf) at 4 °C and washed in 20 mL ice cold ST buffer (20 mM Tris, 200 mM NaCl, pH 8.0), followed by a second centrifugation. The bacteria were resuspended in 5 mL ST buffer and stored at -20 °C. Later, the bacteria were thawed on ice and 5 mg Lysozyme, 1 µl Benzonase (25 U/µl) and 50 µl Halt Protease Inhibitor were added (10320015, Thermo Fisher Scientific). From now on, all steps were performed on ice or at 4 °C. The mixture was incubated for at least 30 min followed by addition of 50 µl of 20% Nonidet-P40. The solution was centrifuged for 30 min at 40062 ×g (Sorval Lynx 6000, Thermo Fisher Scientific) and loaded on 1 mL (bed volume) freshly prepared Ni-NTA resin, according to manufacturers' instructions (88221, Thermo Fisher Scientific). After 1 hour incubation while gently rotating, the beads were washed 7 times with 14 mL ST buffer, each time collecting the beads by centrifugation for 2 min at 700 ×g. The proteins were eluted once with 0.5mL ST buffer with 0.6 M imidazole, and a second and third time with 0.5 mL ST buffer with 0.2 M imidazole.
Salt was removed from the isolated proteins by PD10 desalting columns (17-0851-01, Cytiva), according to manufacturers' instructions. Small salts and molecules (imidazole) flow faster through the column than the large proteins. The columns were equilibrated with 10 mM Tris-HCl pH 8.0 before loading, and proteins were eluted with the same buffer. The visually brightest fractions were collected. For storage, aliquots were snap-frozen in liquid nitrogen and stored at -80 °C.

Quantum yield. The quantum yield (QY) was determined by measuring the absorbance and emission spectra of a range of dilutions of purified G-Ca-FLITS or Tq-Ca-FLITS_T203Y in 1 mL 0 or 39 µM free Ca^{2+} buffer of Calcium Calibration Buffer Kit #1 (C3008MP, Thermo Fisher Scientific). In addition, mTq2_T203Y was measured diluted in a 10 mM Tris-HCl buffer (pH 8.0). First, a quartz cuvette was filled with 1 mL of the required buffer and the absorbance spectrum (250 - 550 nm, 1 nm step size) was measured using a spectrophotometer (Libra S70, Biochrom). The cuvette was transferred to a JASCO FP-8500 spectrofluorometer and the emission spectrum was recorded at 460 - 700 nm with a 2.5 nm bandwidth and 1 nm intervals, while exciting at 450 nm with 2.5 nm bandwidth, using a scan speed of 500 nm/min, 1 s response time and a medium sensitivity. A small amount of purified protein was added, and the absorbance and emission spectra were recorded again. This was repeated for in total 4 dilutions per protein and while the absorbance at 450 nm was always below 0.05 for the highest concentration. An additional absorbance spectrum was recorded with a peak absorbance "A_{peak}" of 0.5. The same procedure was followed for rhodamine as a reference in 1 mM NaOH.

Absorbance spectra were corrected by subtraction of the offset of the spectrum between 541 and 550 nm, followed by subtraction of the spectrum of only buffer. The resolution of the spectrophotometer is too low for the low protein levels, so the resulting spectra are not smooth. Therefore, the additionally taken absorbance spectrum with A_{peak} = 0.5 were fitted to the low-resolution spectra. From this fit, the absorbance at 450 nm (A_{450}) was determined for each dilution of protein. Emission spectra were corrected for spectral sensitivity of the detector and the spectrum of the only buffer sample was subtracted. The spectral area "I_{em}" under corrected emission spectra was calculated by integration between 460 - 700 nm.
The "A_{450}" was plotted versus "I_{em}" and the slope *"s"* was determined while forcing the regression line through the origin: $A_{450} = s \times I_{\mathrm{em}}$. The regression was performed in R studio (version 1.0.136), using the linear model form the stats package with default parameters. The Quantum Yield (QY_s) of the protein samples was determined according to:

$$QY_s = QY_r \times \frac{s_s}{s_r} \quad (1)$$

where subscripts "*s*" and "*r*" indicate the protein sample and the reference rhodamine, QY_r = 0.85 (Zhang et al., 2014), respectively. The standard deviation in "QY_s" was determined from the standard deviation of "s_s".

Extinction coefficient. Purified G-Ca-FLITS, Tq-Ca-FLITS_T203Y and mTq2_T203Y were ~10× diluted in calcium buffers containing 0 or 39 µM free calcium of the Calcium Calibration Buffer Kit #1 (C3008MP, Thermo Fisher Scientific) to a final volume of 200 µL. The absorbance spectra were measured before and after addition of 0.5 M NaOH and 2M urea, at 260 - 650 nm with 1 nm step size and 1 nm bandwidth. Corresponding buffer was used as reference. The concentration of unfolded protein was determined using the Beer-Lambert law and assuming an extinction coefficient (ε) at 462 nm of 46 mM^{-1} cm^{-1} for the free cyan chromophore (Lelimousin et al., 2009). Next, ε_{max} was determined at maximum absorbance for G-Ca-FLITS, Tq-Ca-FLITS_T203Y and mTq2_T203Y.

***In vitro* calibration**. Purified G-Ca-FLITS were diluted 1000× in calcium buffers ranging from 0 to 39 µM, using the Calcium Calibration Buffer Kit #1 according to manufacturers' instructions. Dilutions were made in triplicate in a 96-well plate with black walls and flat glass bottom (89626, Ibidi). Fluorescence lifetime was recorded of each well as described under '**lifetime imaging'**, first at RT and later at 37 °C, using the same plate. The average phase and modulation lifetime (τ_ϕ and τ_M) of the full view were determined per well. The average τ_ϕ and τ_M were determined for 0 and 39 µM free Ca^{2+}, these are "min" and "max". The Phase (Φ) and modulation (*M*) were calculated from the recorded lifetimes and displayed in a polar plot as *G* and *S* coordinates:

$$\Phi = \mathrm{atan}\,(\omega\tau_\varphi) \quad \text{and} \quad M = \sqrt{\frac{1}{1+(\omega\,\tau_{\mathrm{M}})^2}}$$
$$G = M\cos(\Phi) \quad \text{and} \quad S = M\sin(\Phi) \quad (2)$$

The angular frequency of modulation, $2\pi f$, is given by "ω", and we used f = 40 MHz. Measurements were projected on the straight line between the two extremes ("min" and "max") and converted to line fraction "*a*" (equation 3).

$$dG = G - G_{\min} \quad \text{and} \quad dS = S - S_{\min}$$

$$a = \frac{dG \times dG_{\max} + dS \times dS_{\max}}{{dG_{\max}}^2 + {dS_{\max}}^2} \tag{3}$$

The line fraction was corrected of for the intensity contribution of the two states to find the true fraction "*F*", with *F* = 1 representing all sensors in the calcium-bound state (Eq. 4). The intensity ratio (*R*) between states in vitro was determined to be *R* = 0.836, based on the theoretical ratio calculated from the spectra of the sensor and the instrument settings, see Supplemental note 1).

$$F = \frac{a}{R \times (1-a) + a} \tag{4}$$

The fraction "*F*" was fitted with the Hill equation (equation 5) to find the in vitro K_d, using the Nonlinear Least Squares method of the R Stats Package (version 3.3.3) in R Studio (version 1.0.136), using the port algorithm.

$$F = F_{\min} + \frac{(F_{\max} - F_{\min})}{\left(\frac{K_d}{L}\right)^n + 1} \tag{5}$$

The microscopic dissociation constant is given by "K_d", the known free Ca^{2+} concentration by "*L*" and the Hill coefficient by "*n*".
The 95% confidence interval (CI) of the fraction of the two extremes was determined from the data. The mean of the low calcium state plus the CI was determined to be the lowest measurable fraction, the mean of the high calcium state minus the CI was determined to be the highest measurable fraction. From this, the lowest and highest measurable concentration was determined using the Hill equation (equation 5).

pH sensitivity. A series of buffers ranging from pH 2.8 to 10.1 were prepared, using 50 mM citrate buffer (pH 2.8 - 5.8), MOPS buffer (pH 6.3 - 7.9) and glycine/NaOH buffer (pH 8.2 - 10.1). Buffers additionally contain 0.1 M KCl and 0.1 mM $CaCl_2$ or 5 mM EGTA. The pH of each buffer was determined including all components shortly before use. Purified G-Ca-FLITS or mTq2_T203Y was diluted 520× in the prepared buffers, using a predilution of 40× and a total volume of 200 µL. The dilutions were made in triplicate in a 96-well plate with black walls and flat glass bottom (89626, ibidi). The lifetime of each well in the same 96-well plate was recorded at RT, see **'Lifetime imaging.'**

Ratiometric imaging. HeLa cells co-expressing a green calcium sensor (or green FP) and mScarlet-I form a single plasmid (pFR) were imaged 24 h after transfection at 37 °C, using an Eclipse Ti microscope (Nikon) equipped with a Spectra X Light Engine (Lumencor) for excitation and an Orca flash 4.0 camera (Hamamatsu). Cells were imaged using a Plan Apo ×10 NA 0.45 air objective. For imaging of GFP, a 470 nm LED, a 470/24 nm excitation filter and a quad band cube (MXU 71640, Nikon) were used. For RFP, a 575 nm LED, a 575/25 nm excitation filter and the same quad band cube were used. Only the middle of the field of view was used, to minimize the unequal illumination. A 4x4 tile scan was performed and channels were imaged sequentially.
Fluorescence was recorded without stimulation and directly after stimulation with a mix of ionomycin (5 µg/mL, I-6800, LClaboratories) and calcium (5 mM). Background was subtracted

from the images and the average green and red fluorescence intensity of individual cells was measured using ImageJ (version 1.52k). The ratio GFP/RFP was calculated for each cell. As a control, we used a sample with only mScarlet-I (ratio GFP/RFP = 0) and a sample with EGFP and mScarlet-I (ratio GFP/RFP = 1). The ratio of all cells was normalized to the controls. The experiment was performed twice per construct.

Confocal imaging. Confocal images of HeLa cells and BOECs expressing G-Ca-FLITS were taken with a Leica Sp8 system (Leica) with a ×63 objective (HL PL Apo, C2S NA 1.40 oil) at 37 °C and 7% (HeLa cells) or 5% CO_2 (BOECs). HeLa cells were imaged in MM and BOECs in growth medium, as stated before. A 488 nm Argon laser was used for imaging, combined with an Acousto-Optical Beam Splitter (AOBS), and fluorescence was collected with a HyD at 500 - 780 nm. The pinhole was set to 1 AU.

Confocal TCSPC imaging - Picoharp TCSPC module. Confocal fluorescence lifetime images of G-Ca-FLITS expressed in mitochondria of Hela cells were acquired at an FV1000 (Olympus) confocal microscope equipped with a Picoharp TCSPC module (PicoQuant). A field of view of 256x256 pixels (207 - 331 nm per pixel) was illuminated with a pulsed 485 nm Picoquant diode laser (20 MHz, 0.4 $kW \cdot cm^{-2}$) using an Olympus UPLS Apo 60x water NA1.2 objective lens. The fluorescence signal was detected in confocal mode with the pinhole diameter set at 130 µm. The fluorescence passed a 405/480/560/635 dichroic mirror, was filtered by a 505 - 540 nm emission filter and detected by avalanche photodiodes (MPD).
In order, to obtain a reliable fluorescence lifetime the measurement times of the sample channel was set such that at least 10^5 photons were collected. An image of the median arrival times per pixel was inspected for heterogeneity. Based on the image, one or more regions were manually selected for fitting of a decay curve. The full fluorescence decay curves (5-6 minutes integration time) were fitted in the Symphotime64 software (PicoQuant) using a bi-exponential decay model including an instrumental response function generated from the same dataset. On basis of visual inspection of the fit, the fit residuals and the minimal Chi square the fitted results were accepted or discarded. The fitting of the decay curves was repeated for all areas, but now an integration time of 1 minute was used. The fitting was repeated for every minute, to obtain information about temporal variation.

Confocal TCSPC imaging – Leica Stellaris. Confocal fluorescence lifetime images of G-Ca-FLITS expressed in mitochondria of Hela cells were acquired with a Leica Stellaris8 equipped with a pulsed white light laser set to 40 MHz and a 40x NA 0.95 air PL APO objective. The excitation was at 474 nm and the emission was detected between 490 nm and 600 nm by the HyDX2 detector. The pinhole was set to 4.4 airy units, the imaging speed to 400 Hz per line (pixel dwell time 3.16 µs) with 8 line repetitions and a frame size of 512x512 (pixel size 0.259 µm). For live-cell imaging, the images were acquired every minute.
The data was saved as .ptu file and a custom script was used to convert these data into G and S images. The G and S data, together with the K_D determined by the calibration, were used to convert the data into calcium concentration.

Imaging and analysis of 2P-FLIM of Drosophila
We imaged the brain of *Drosophila melanogaster* females attached to a custom physiology platform (Maimon et al, 2010, Mussells Pires et al., 2024). This platform keeps the fly's body dry and in air, with the brain exposed to an experimentally determined saline. The flies were

freely dangling and we did not track their behavior. We removed the superior cuticle of the head (the frons and anterior ocellar cuticle) to access the brain dorsally for optical imaging.
Extracellular saline was prepared as reported (Mussells Pires et al., 2024), consisting of (in mM): 103 NaCl, 3 KCl, 5 TES, 10 trehalose dihydrate, 10 glucose, 2 sucrose, 26 $NaHCO_3$, 1 NaH_2PO_4, 1.5 $CaCl_2$ and 4 $MgCl_2$ titrated with Milli-Q water to an osmolarity of 280-285 mOsm. The high [K+] solution exchanged the concentrations of NaCl with KCl, keeping the osmolarity and [Cl-] unchanged.
The saline was kept at ~21°C for the duration of all experiments using a Warner Instruments temperature controller (CL-100) driving a Peltier device (SC-20). The Peltier device was placed in-line with tubing (Tygon 2375) that perfused the preparation with saline at a rate of ~3 mL per minute. A thermistor in the bath was used to regulate the Peltier device in closed loop.
The high [K+] solution was applied by allowing flow through the perfusion line to exchange with the extracellular solution, which was gradually aspirated out of the chamber using a glass pipette attached to a vacuum. Each recording was given ~10 minutes to respond to the new solution and we estimate that the saline composition of the preparation was fully replaced within ~1 min.
The 2P-FLIM setup uses an Olympus 20x 1.0 NA water immersion objective (XLUMPLFLN) on a customized Sutter MIMMs to be detailed in a later manuscript by SCT and GM. A Coherent Discovery NX laser's tunable beam set to 920 nm (with -12,500 fs2 of dispersion compensation) was used to excite all three fluorophores.
Frames were collected at a resolution of 256 x 256 pixels and the time series data shown in Figure 8 are plotted at ~1 Hz. Flies expressing jGCaMP7f or Tq-Ca-FLITS were imaged with ~20 mW of laser power measured after the objective, while flies expressing G-Ca-FLITS were imaged with ~30 mW laser power.
The fluorescence lifetime was computed by fitting the first 1200 frames to a biexponential distribution convolved with a Gaussian plus randomly distributed uniform noise by minimizing the chi-squared statistic (Thornquist et al., 2020). The offset of this fit was used to adjust the mean photon arrival time within each frame (empirical lifetime), and the contribution of the estimated noise was subtracted out. Explicitly, the arrival time histogram was fit to the equation:

$$p(t) = \epsilon + f_1 F_1(t;\ \tau_1, \sigma, \mu) + f_2 F_2(t;\ \tau_2, \sigma, \mu) \tag{6}$$

where

$$F(t; \tau, \sigma, \mu) = \sqrt{\frac{\pi\sigma^2}{2\tau^2}} \exp\left(\frac{\sigma^2}{2\tau^2}\right) \operatorname{erfc}\left(\frac{1}{\sqrt{2}}\left(\frac{\sigma}{\tau} - \frac{t-\mu}{\sigma}\right)\right) \exp\left(-\frac{t-\mu}{\tau}\right) \tag{7}$$

is the single exponential response with a time constant τ convolved with a Gaussian centered at μ with standard deviation σ and $\epsilon + f_1 + f_2 = 1$. To compute the empirical lifetime L of a collection of photons we computed the mean arrival time of the photons $\langle p \rangle = \sum_{t=0}^{t_{max}} t * p(t)$, then removed the offset and the estimated noise due to the uniform signal (which had mean arrival time $\frac{t_{max}}{2}$ because it is uniformly distributed):

$$L = \langle p \rangle - \left(\mu + \epsilon \frac{t_{max}}{2}\right) \tag{8}$$

Mean intensity-weighted lifetime refers to the following procedure: when taking the mean of a set of n frames, the lifetime was computed as

$$\langle L \rangle = \sum_{k=1}^{n} \frac{I_k L_k}{n \langle I \rangle} \tag{9}$$

where I_k refers to the intensity of the kth frame, L_k refers to the mean lifetime of the kth frame, and $\langle \circ \rangle$ refers to the average across frames.

Data availability

Several plasmids are deposited for distribution through Addgene (www.addgene.org). The plasmids and corresponding addgene numbers are: N1-G-Ca-FLITS: #191465, 3xnls-G-Ca-FLITS: #191463, 4xmts-G-Ca-FLITS: #191462, ER-G-Ca-FLITS-KDEL: #191464, pFPO-His-mTurquoise2_T203Y: #191456, pFPO-His-G-Ca-FLITS: #191455, pFR-mScarletI-antiFRET-P2A-G-Ca-FLITS: #191457, pFR-mScarletI-antiFRET-P2A-EGFP: #191458, pFR-mScarletI-antiFRET-P2A-mTurquoise2_T203Y: #191459, pFR-mScarletI-antiFRET-P2A-GCaMP3: #191460, pFR-mScarletI-antiFRET-P2A-jGCaMP7c: #191461, pDress-mScarletI-antiFRET-P2A2-linker_noSacI: #191473. Transgenic Drosophila lines expressing Tq-Ca-FLITS under UAS or LexA control and G-Ca-FLITS under UAS control are available upon request.
Data and code will be made available upon publication.

Acknowledgements

F.H.L. was supported by a NWO Chemical Sciences ECHO grant (711.017.003). G.M. is a Howard Hughes Medical Institute Investigator. The funder(s) had no role in study design, data collection and analysis, decision to publish, or preparation of the manuscript.

Competing interests

The authors declare no competing interests.

Author contributions

F.H.L. and J.G. conceptualized the project, designed the experiments, interpreted the results, and wrote the manuscript. F.H.L. engineered and characterized the green biosensor, and tested it in mammalian cells. S.C.T. and G.M. performed experiments on *Drosophila*, analysed the data and prepared text and figures. R.M.B. and J.Y.H. were involved in the engineering of the green biosensor and setting up the screen. M.H. assisted with TCSPC FLIM imaging and processing of the data. T.W.J.G. assisted in FLIM data processing, analysis, and interpretation of the data. All authors approved the final manuscript.

References

Akerboom J, Carreras Calderón N, Tian L, Wabnig S, Prigge M, Tolö J, Gordus A, Orger MB, Severi KE, Macklin JJ, Patel R, Pulver SR, Wardill TJ, Fischer E, Schüler C, Chen T-W, Sarkisyan KS, Marvin JS, Bargmann CI, Kim DS, Kügler S, Lagnado L, Hegemann P, Gottschalk A, Schreiter ER, Looger LL. 2013. Genetically encoded calcium indicators for multi-color neural activity imaging and combination with optogenetics. *Frontiers in Molecular Neuroscience* **6**:1–29. doi:10.3389/fnmol.2013.00002

Arnaudeau S, Kelley WL, Walsh JV, Demaurex N. 2001. Mitochondria Recycle Ca2+ to the Endoplasmic Reticulum and Prevent the Depletion of Neighboring Endoplasmic Reticulum Regions. *Journal of Biological Chemistry* **276**:29430–29439. doi:10.1074/jbc.M103274200

Barykina NV, Subach OM, Doronin DA, Sotskov VP, Roshchina MA, Kunitsyna TA, Malyshev AY, Smirnov IV, Azieva AM, Sokolov IS, Piatkevich KD, Burtsev MS, Varizhuk AM, Pozmogova GE, Anokhin KV, Subach FV, Enikolopov GN. 2016. A new design for a green calcium indicator with a smaller size and a reduced number of calcium-binding sites. *Scientific Reports* **6**:1–15. doi:10.1038/srep34447

Bastiaens PIH, Wolkers WF, Visser AJWG, Van Hoek A, Brochon JC. 1992. Comparison of the Dynamical Structures of Lipoamide Dehydrogenase and Glutathione Reductase by Time-Resolved Polarized Flavin Fluorescence. *Biochemistry* **31**:7050–7060. doi:10.1021/bi00146a005

Berridge MJ, Lipp P, Bootman MD. 2000. The Versatility and Universality of Calcium Signalling. *Nature Reviews* **1**:11–21. doi:10.1038/35036035

Bierbuesse F, Bourges AC, Gielen V, Mönkemöller V, Vandenberg W, Shen Y, Hofkens J, Berghe PV, Campbell RE, Moeyaert B, Dedecker P. 2022. Absolute measurement of cellular activities using photochromic single-fluorophore biosensors and intermittent quantification. *Nature Communications* **13**:1–13. doi:10.1038/s41467-022-29508-w

Bindels DS, Goedhart J, Hink MA, Weeren LV, Joosen L, Gadella TWJ. 2014. Chapter 16: Optimization of Fluorescent ProteinsFluorescence Spectroscopy and Microscopy. pp. 371–417. doi:10.1007/978-1-62703-649-8

Bindels DS, Postma M, Haarbosch L, van Weeren L, Gadella TWJ. 2020. Multiparameter screening method for developing optimized red-fluorescent proteins. *Nature Protocols* **15**:450–478. doi:10.1038/s41596-019-0250-7

Boens N, Wenwu Q, Basarić N, Hofkens J, Ameloot M, Pouget J, Lefévre J-P, Valeur B, Gratton E, VandeVen M, Silva ND, Engelborghs Y, Willaert K, Sillen A, Bumbles G, Phillips D, Visser AJWG, van Hoek A, Lakowicz JR, Malak H, Gryczynski I, Szabo AG, Krajcarski DT, Tamai N, Miura A. 2007. Fluorescence Lifetime Standards for Time and Frequency Domain Fluorescence Spectroscopy. *Analytical Chemistry* **79**:2137–2149. doi:10.1021/ac062160k

Cano Abad MF, Di Benedetto G, Magalhães PJ, Filippin L, Pozzan T. 2004. Mitochondrial pH Monitored by a New Engineered Green Fluorescent Protein Mutant. *Journal of Biological Chemistry* **279**:11521–11529. doi:10.1074/jbc.M306766200

Chen TW, Wardill TJ, Sun Y, Pulver SR, Renninger SL, Baohan A, Schreiter ER, Kerr RA, Orger MB, Jayaraman V, Looger LL, Svoboda K, Kim DS. 2013. Ultrasensitive fluorescent proteins for imaging neuronal activity. *Nature* **499**:295–300. doi:10.1038/nature12354

Collins TJ, Berridge MJ, Lipp P, Bootman MD. 2002. Mitochondria are morphologically and functionally heterogeneous within cells. *EMBO Journal* **21**:1616–1627. doi:10.1093/emboj/21.7.1616

Culley S, Caballero AC, Burden JJ, Uhlmann V. 2024. Made to measure: An introduction to quantifying microscopy data in the life sciences. *Journal of Microscopy* **295**:61–82. doi:10.1111/jmi.13208

Dalal PJ, Muller WA, Sullivan DP. 2020. Endothelial Cell Calcium Signaling during Barrier Function and Inflammation. *American Journal of Pathology* **190**:535–542. doi:10.1016/j.ajpath.2019.11.004

Dana H, Sun Y, Mohar B, Hulse BK, Kerlin AM, Hasseman JP, Tsegaye G, Tsang A, Wong A, Patel R, Macklin JJ, Chen Y, Konnerth A, Jayaraman V, Looger LL, Schreiter ER, Svoboda K, Kim DS. 2019. High-performance calcium sensors for imaging activity in neuronal populations and microcompartments. *Nature Methods* **16**:649–657. doi:10.1038/s41592-019-0435-6

Danilevich VN, Petrovskaya LE, Grishin EV. 2008. A Highly Efficient Procedure for the Extraction of Soluble Proteins from Bacterial Cells with Mild Chaotropic Solutions. *Chemical Engineering & Technology* **31**:904–910. doi:10.1002/ceat.200800024

Delierneux C, Kouba S, Shanmughapriya S, Potier-Cartereau M, Trebak M, Hempel N. 2020. Mitochondrial Calcium Regulation of Redox Signaling in Cancer. *Cells* **9**:1–24. doi:10.3390/cells9020432

Díaz-García CM, Mongeon R, Lahmann C, Koveal D, Zucker H, Yellen G. 2017. Neuronal Stimulation Triggers Neuronal Glycolysis and Not Lactate Uptake. *Cell Metabolism* **26**:361–374. doi:10.1016/j.cmet.2017.06.021

Fernandez-Sanz C, De la Fuente S, Sheu S-S. 2019. Mitochondrial Ca2+ concentrations in live cells: quantification methods and discrepancies. *FEBS Letters* **593**:1528–1541. doi:10.1002/1873-3468.13427

Fonteriz RI, de la Fuente S, Moreno A, Lobatón CD, Montero M, Alvarez J. 2010. Monitoring mitochondrial [Ca2+] dynamics with rhod-2, ratiometric pericam and aequorin. *Cell Calcium* **48**:61–69. doi:10.1016/j.ceca.2010.07.001

Gadella TWJ. 2009. Fret and Flim Techniques, Laboratory Techniques in Biochemistry and Molecular Biology.

Gadella TWJ, Clegg RM, Jovint TM. 1994. Fluorescence lifetime imaging microscopy: pixel-by-pixel analysis of phase-modulation data. *Bioimaging* **2**:139–159.

García-Nafría J, Watson JF, Greger IH. 2016. IVA cloning: A single-tube universal cloning system exploiting bacterial In Vivo Assembly. *Scientific Reports* **6**:27459. doi:10.1038/srep27459

Giorgi C, Marchi S, Pinton P. 2018. The machineries, regulation and cellular functions of mitochondrial calcium. *Nature Reviews Molecular Cell Biology* **19**:713–730. doi:10.1038/s41580-018-0052-8

Gorbachev DA, Sarkisyan KS, Mishin AS, Lukyanov KA. 2017. Green fluorescent protein with tryptophan-based chromophore stable at low pH. *Russian Journal of Bioorganic Chemistry* **43**:220–222. doi:10.1134/S1068162017010034

Green J, Vijayan V, Mussells Pires P, Adachi A, Maimon G. 2019. A neural heading estimate is compared with an internal goal to guide oriented navigation. *Nature Neuroscience* **22**:1460–1468. doi:10.1038/s41593-019-0444-x

Greenwald EC, Mehta S, Zhang J. 2018. Genetically Encoded Fluorescent Biosensors Illuminate the Spatiotemporal Regulation of Signaling Networks. *Chem Rev* **118**:11707–11794. doi:10.1021/acs.chemrev.8b00333

Greotti E, Fortunati I, Pendin D, Ferrante C, Galla L, Zentilin L, Giacca M, Kaludercic N, Di Sante M, Mariotti L, Lia A, Gómez-Gonzalo M, Sessolo M, Carmignoto G, Bozio R, Pozzan T. 2019. mCerulean3-Based Cameleon Sensor to Explore Mitochondrial Ca2+ Dynamics In Vivo. *iScience* **16**:340–355. doi:10.1016/j.isci.2019.05.031

Kim JH, Lee SR, Li LH, Park HJ, Park JH, Lee KY, Kim MK, Shin BA, Choi SY. 2011. High cleavage efficiency of a 2A peptide derived from porcine teschovirus-1 in human cell lines, zebrafish and mice. *PLoS ONE* **6**:1–8. doi:10.1371/journal.pone.0018556

Klarenbeek J, Goedhart J, van Batenburg A, Groenewald D, Jalink K. 2015. Fourth-Generation Epac-Based FRET Sensors for cAMP Feature Exceptional Brightness, Photostability and Dynamic Range: Characterization of Dedicated Sensors for FLIM, for Ratiometry and with High Affinity. *PLoS One* **10**. doi:10.1371/journal.pone.0122513

Koveal D, Rosen PC, Meyer DJ, Díaz-García CM, Wang Y, Cai L-H, Chou PJ, Weitz DA, Yellen G. 2022. A high-throughput multiparameter screen for accelerated development and optimization of soluble genetically encoded fluorescent biosensors. *Nat Commun* **13**:2919. doi:10.1038/s41467-022-30685-x

Laskaratou D, Fernández GS, Coucke Q, Fron E, Rocha S, Hofkens J, Hendrix J, Mizuno H. 2021. Quantification of FRET-induced angular displacement by monitoring sensitized acceptor anisotropy using a dim fluorescent donor. *Nature Communications* **12**:1–12. doi:10.1038/s41467-021-22816-7

Lelimousin M, Noirclerc-Savoye M, Lazareno-Saez C, Paetzold B, Le Vot S, Chazal R, Macheboeuf P, Field MJ, Bourgeois D, Royant A. 2009. Intrinsic dynamics in ECFP and cerulean control fluorescence quantum yield. *Biochemistry* **48**:10038–10046. doi:10.1021/bi901093w

Liu Z, Chen O, Wall JBJ, Zheng M, Zhou Y, Wang L, Ruth Vaseghi H, Qian L, Liu J. 2017. Systematic comparison of 2A peptides for cloning multi-genes in a polycistronic vector. *Scientific Reports* **7**:1–9. doi:10.1038/s41598-017-02460-2

Llopis J, McCaffery JM, Miyawaki A, Farquhar MG, Tsien RY. 1998. Measurement of cytosolic, mitochondrial, and Golgi pH in single living cells with green fluorescent proteins. *Proceedings of the National Academy of Sciences* **95**:6803–6808. doi:10.1073/pnas.95.12.6803

Maimon G, Straw AD, Dickinson MH. 2010. Active flight increases the gain of visual motion processing in Drosophila. *Nature Neuroscience* **13**:393–399. doi:10.1038/nn.2492

Martin-Ramirez J, Hofman M, Van Den Biggelaar M, Hebbel RP, Voorberg J. 2012. Establishment of outgrowth endothelial cells from peripheral blood. *Nature Protocols* **7**:1709–1715. doi:10.1038/nprot.2012.093

Molina RS, Tran TM, Campbell RE, Lambert GG, Salih A, Shaner NC, Hughes TE, Drobizhev M. 2017. Blue-Shifted Green Fluorescent Protein Homologues Are Brighter than Enhanced Green Fluorescent Protein under Two-Photon Excitation. *J Phys Chem Lett* **8**:2548–2554. doi:10.1021/acs.jpclett.7b00960

Mussells Pires P, Zhang L, Parache V, Abbott LF, Maimon G. 2024. Converting an allocentric goal into an egocentric steering signal. *Nature* **626**:808–818. doi:10.1038/s41586-023-07006-3

Ngo J, Osto C, Villalobos F, Shirihai OS. 2021. Mitochondrial heterogeneity in metabolic diseases. *Biology* **10**:1–25. doi:10.3390/biology10090927

Ormö M, Cubitt AB, Kallio K, Gross LA, Tsien RY, Remington J. 1996. Crystal structure of the Aequorea victoria green fluorescent protein. *Science* **273**. doi:10.1126/science.273.5280.1392

Palmer AE, Giacomello M, Kortemme T, Hires SA, Lev-Ram V, Baker D, Tsien RY. 2006. Ca2+ Indicators Based on Computationally Redesigned Calmodulin-Peptide Pairs. *Chemistry and Biology* **13**:521–530. doi:10.1016/j.chembiol.2006.03.007

Park MK, Ashby MC, Erdemli G, Petersen OH, Tepikin AV. 2001. Perinuclear, perigranular and sub-plasmalemmal mitochondria have distinct functions in the regulation of cellular calcium transport. *EMBO Journal* **20**:1863–1874. doi:10.1093/emboj/20.8.1863

Parry HA, Willingham TB, Giordano KA, Kim Y, Qazi S, Knutson JR, Combs CA, Glancy B. 2024. Impact of capillary and sarcolemmal proximity on mitochondrial structure and energetic function in skeletal muscle. *The Journal of Physiology* **602**:1967–1986. doi:10.1113/JP286246

Rotrosen D, Gallin JI. 1986. Histamine type i receptor occupancy increases endothelial cytosolic calcium, reduces f-actin, and promotes albumin diffusion across cultured endothelial monolayers. *Journal of Cell Biology* **103**:2379–2387. doi:10.1083/jcb.103.6.2379

Rusinova E, Tretyachenko-Ladokhina V, Vele OE, Senear DF, Alexander Ross JB. 2002. Alexa and Oregon Green dyes as fluorescence anisotropy probes for measuring protein-protein and protein-nucleic acid interactions. *Analytical Biochemistry* **308**:18–25. doi:10.1016/S0003-2697(02)00325-1

Seelig JD, Jayaraman V. 2015. Neural dynamics for landmark orientation and angular path integration. *Nature* **521**:186–191. doi:10.1038/nature14446

Shen Y, Dana H, Abdelfattah AS, Patel R, Shea J, Molina RS, Rawal B, Rancic V, Chang YF, Wu L, Chen Y, Qian Y, Wiens MD, Hambleton N, Ballanyi K, Hughes TE, Drobizhev M, Kim DS, Koyama M, Schreiter ER, Campbell RE. 2018. A genetically encoded Ca2+indicator based on circularly permutated sea anemone red fluorescent protein eqFP578. *BMC Biology* **16**:1–16. doi:10.1186/s12915-018-0480-0

Thornquist SC, Langer K, Zhang SX, Rogulja D, Crickmore MA. 2020. CaMKII Measures the Passage of Time to Coordinate Behavior and Motivational State. *Neuron* **105**:334-345.e9. doi:10.1016/j.neuron.2019.10.018

van der Linden FH van der, Mahlandt EK, Arts JJG, Beumer J, Puschhof J, de Man SMA, Chertkova AO, Ponsioen B, Clevers H, van Buul JD, Postma M, Gadella TWJ, Goedhart J. 2021. A turquoise fluorescence lifetime-based biosensor for quantitative imaging of intracellular calcium. *Nature Communications* **12**:7159. doi:10.1038/s41467-021-27249-w

van Munster EB, Gadella TWJ. 2004. Suppression of photobleaching-induced artifacts in frequency-domain FLIM by permutation of the recording order. *Cytometry* **58A**:185–194. doi:10.1002/cyto.a.20013

Waters JC. 2009. Accuracy and precision in quantitative fluorescence microscopy. *Journal of Cell Biology* **185**:1135–1148. doi:10.1083/jcb.200903097

Worthen LM, Nollert MU. 2000. Intracellular calcium response of endothelial cells exposed to flow in the presence of thrombin or histamine. *Journal of Vascular Surgery* **32**:593–601. doi:10.1067/mva.2000.106955

Zhang XF, Zhang Y, Liu L. 2014. Fluorescence lifetimes and quantum yields of ten rhodamine derivatives: Structural effect on emission mechanism in different solvents. *Journal of Luminescence* **145**:448–453. doi:10.1016/j.jlumin.2013.07.066

Zhang Y, Rózsa M, Liang Y, Bushey D, Wei Z, Zheng J, Reep D, Broussard GJ, Tsang A, Tsegaye G, Narayan S, Obara CJ, Lim JX, Patel R, Zhang R, Ahrens MB, Turner GC, Wang SSH, Korff WL, Schreiter ER, Svoboda K, Hasseman JP, Kolb I, Looger LL. 2023. Fast and sensitive GCaMP calcium indicators for imaging neural populations. *Nature* **615**. doi:10.1038/s41586-023-05828-9

Zhao Y, Araki S, Wu J, Teramoto T, Chang YF, Nakano M, Abdelfattah AS, Fujiwara M, Ishihara T, Nagai T, Campbell RE. 2011. An Expanded Palette of Genetically Encoded Ca2+ indicators. *Science* **333**:1888–1891. doi:10.1126/science.1208592

Zheng K, Jensen TP, Rusakov DA. 2018. Monitoring intracellular nanomolar calcium using fluorescence lifetime imaging. *Nat Protoc* **13**:581–597. doi:10.1038/nprot.2017.154

Zhong C, Arai S, Okada Y. 2024. A versatile platform for single fluorescent protein-based fluorescence lifetime biosensors. doi:10.1101/2024.06.29.601303